Journal of Geophysical Research: Solid Earth

Supporting Information for

New Insights into the Rift-to-Drift Process of the Northern South China Sea Constrained by a Three-dimensional OBS Seismic Structure

Jiazheng Zhang[1*], Minghui Zhao[1,6*], Weiwei Ding[2], César R. Ranero[3,4], Valenti Sallares[3], Jinwei Gao[5], Cuimei Zhang[1], Xuelin Qiu[1,6]

[1]Key Laboratory of Ocean and Marginal Sea Geology, South China Sea Institute of Oceanology, Chinese Academy of Sciences, Guangzhou 510301, China.
[2]Key Laboratory of Submarine Geosciences, State Oceanic Administration, Second Institute of Oceanography, Ministry of Natural Resources, Hangzhou 310012, China.
[3]Barcelona Center for Subsurface Imaging, Instituto de Ciéncies del Mar (ICM-CSIC), Barcelona, Spain.
[4]ICREA, Barcelona, Spain
[5]Laboratory of Marine Geophysics and Deep-Sea Georesource, Institute of Deep-sea Science and Engineering, Chinese Academy of Sciences, Sanya 572000, China.
[6]University of Chinese Academy of Sciences, Beijing 100049, China.

Corresponding author: Jiazheng Zhang (jzzhang@scsio.ac.cn) ; Minghui Zhao (mhzhao@scsio.ac.cn)

Contents of this file

Figures S1 to S18.

Introduction

The supplementary figures (Figures S1-S4) display the 3D models of velocity uncertainty and raytracing count, which are used to show the confidence of final 3D Vp model. The supplementary figures (Figures S5-S12) display a set of checkerboard tests mainly showing three different squared cell sizes (4, 10, 20 km), which are used to evaluate the resolution of the tomographic Vp model. The supplementary figures (Figures S13-S16) display the 3D models of velocity gradient and velocity perturbation, which are used to help analyze the final 3D Vp model. The supplementary Figure S17 displays the comparison between 2D and 3D Vp models along L2, which is used to indicate that it is reasonable to take 7.5 km/s velocity contour in our 3D Vp model as the Moho. Figure S18 displays the relationship among HVLC thickness, melt thickness, crustal stretching factor, rifting duration, potential temperature of asthenosphere as well as initial continental lithospheric thickness.

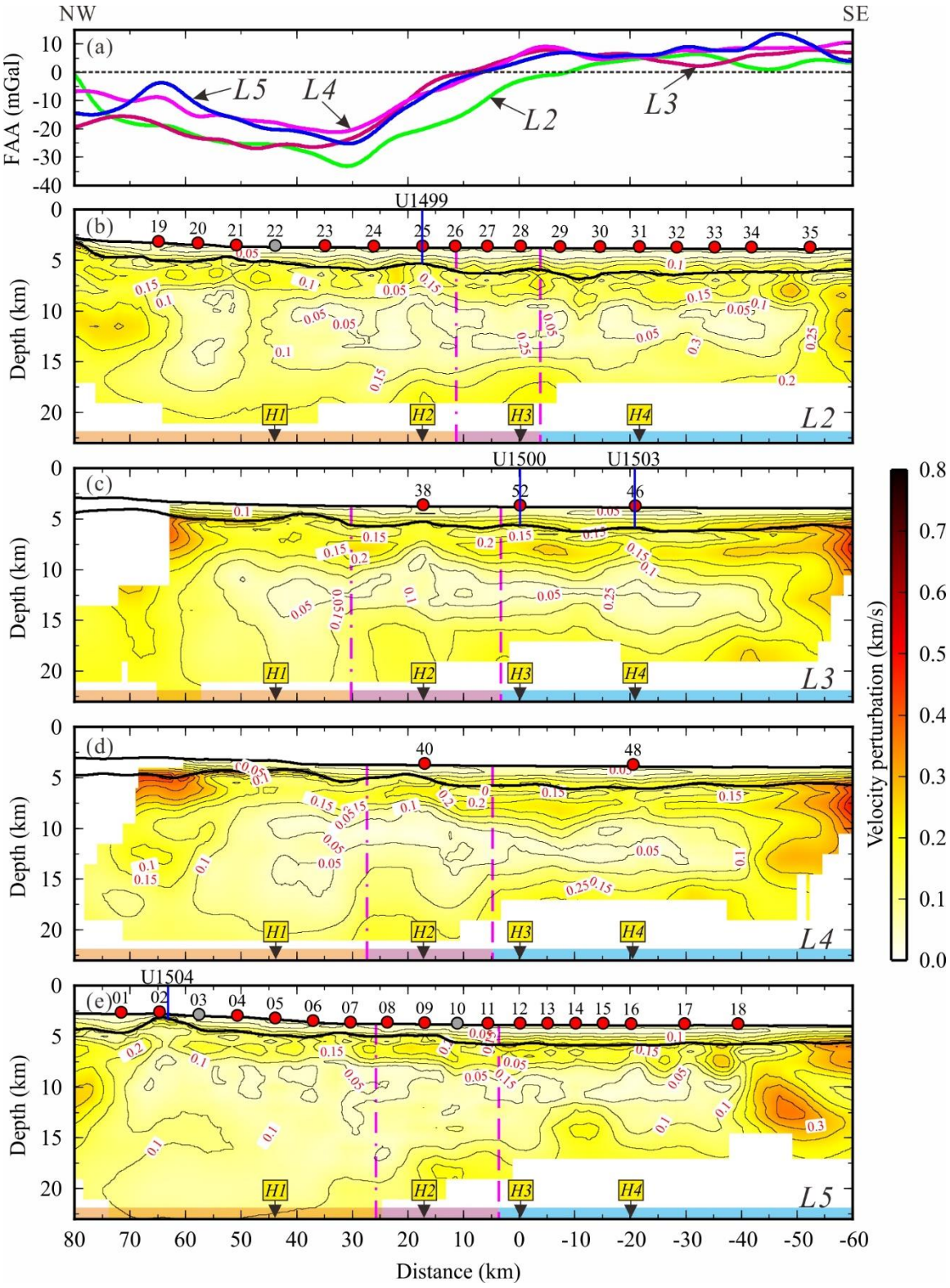

Figure S1. Vertical slices crosscutting the 3D Vp uncertainty model and free-air gravity anomaly. The other symbols are same as Figure 5.

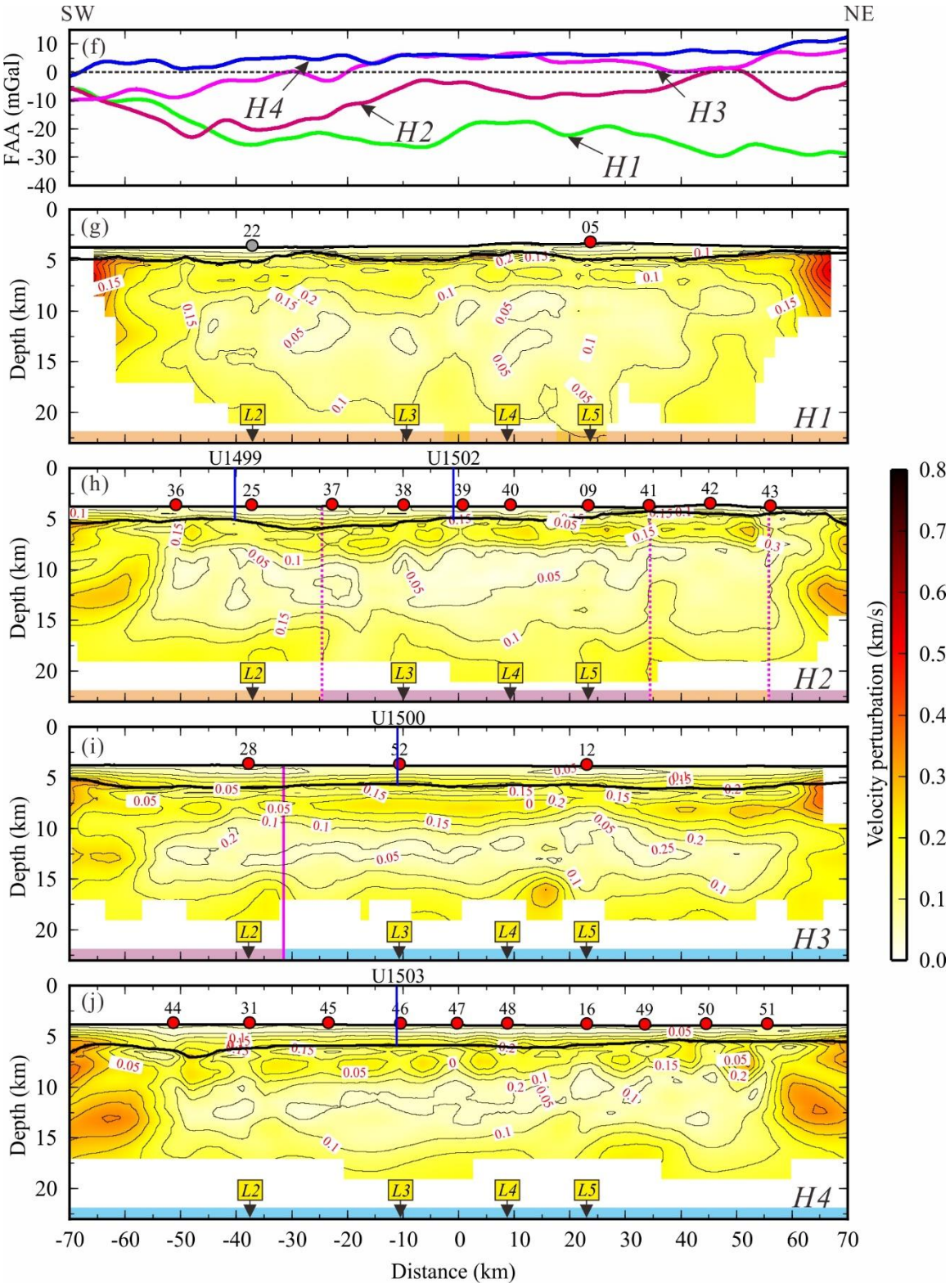

Figure S1 (Continuous).

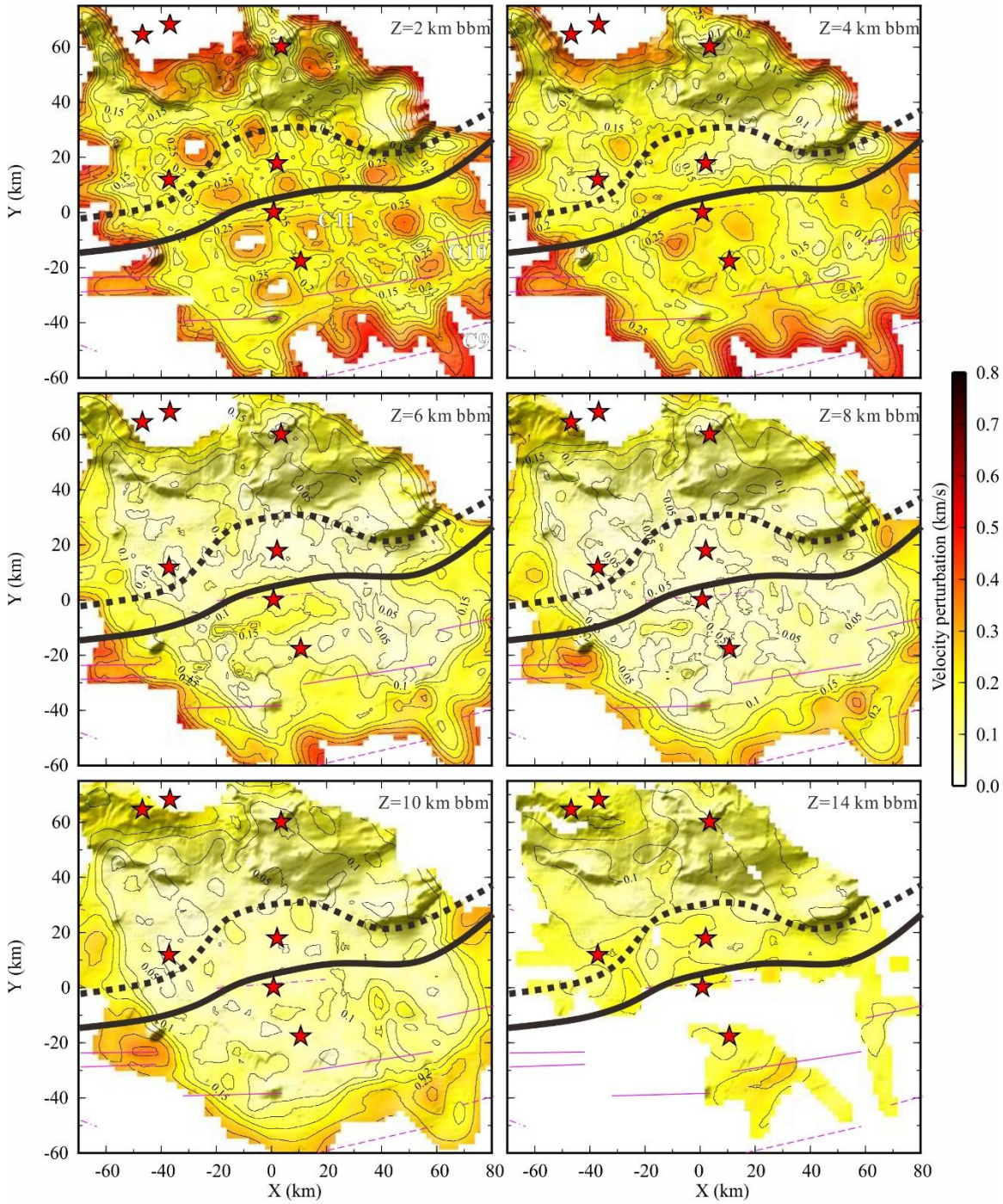

Figure S2. Horizontal slices of the 3D Vp uncertainty model at different depths below TOB (bbm). The other symbols are same as Figure 6.

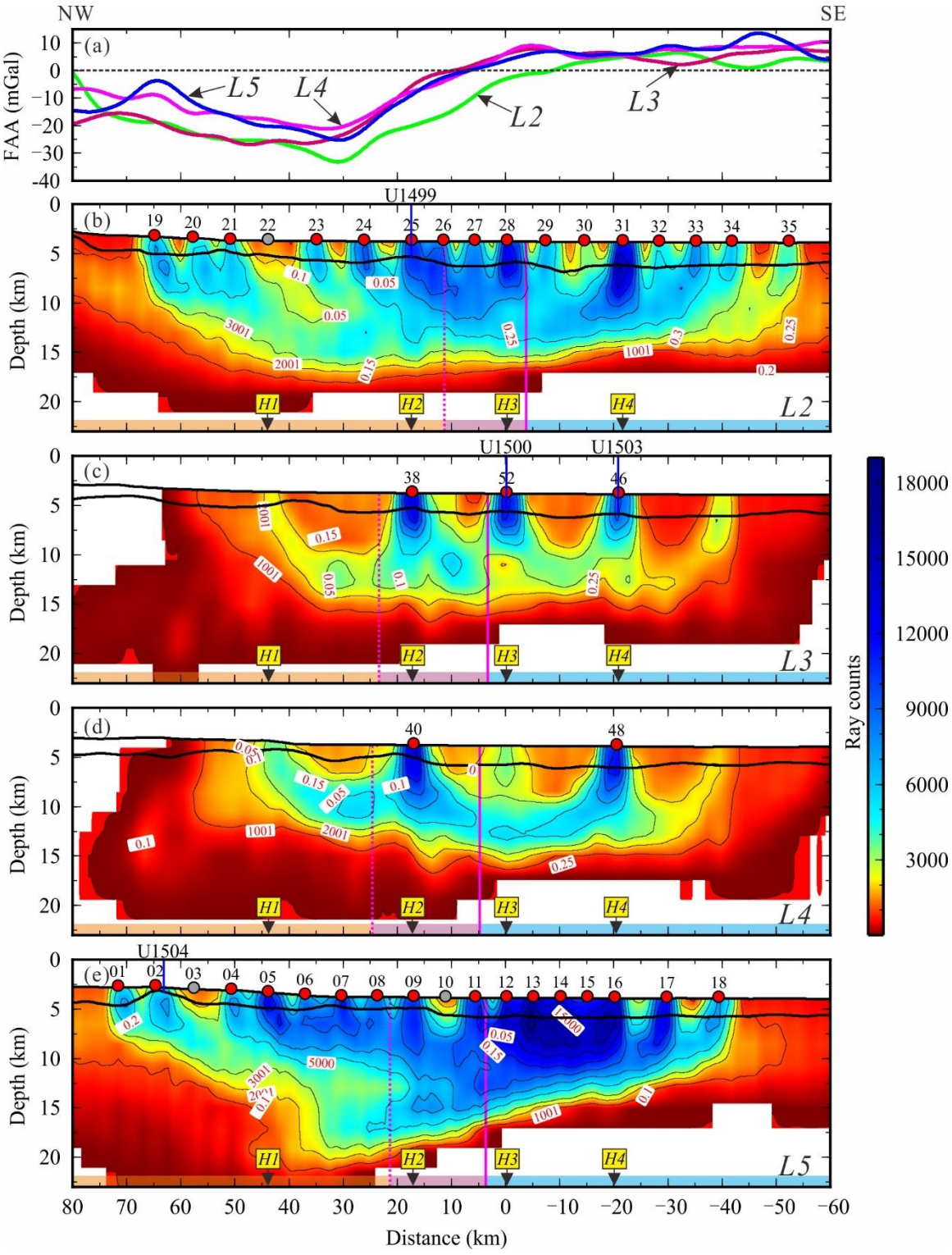

Figure S3. Vertical slices crosscutting the 3D raytracing count model and free-air gravity anomaly. The other symbols are same as Figure 5.

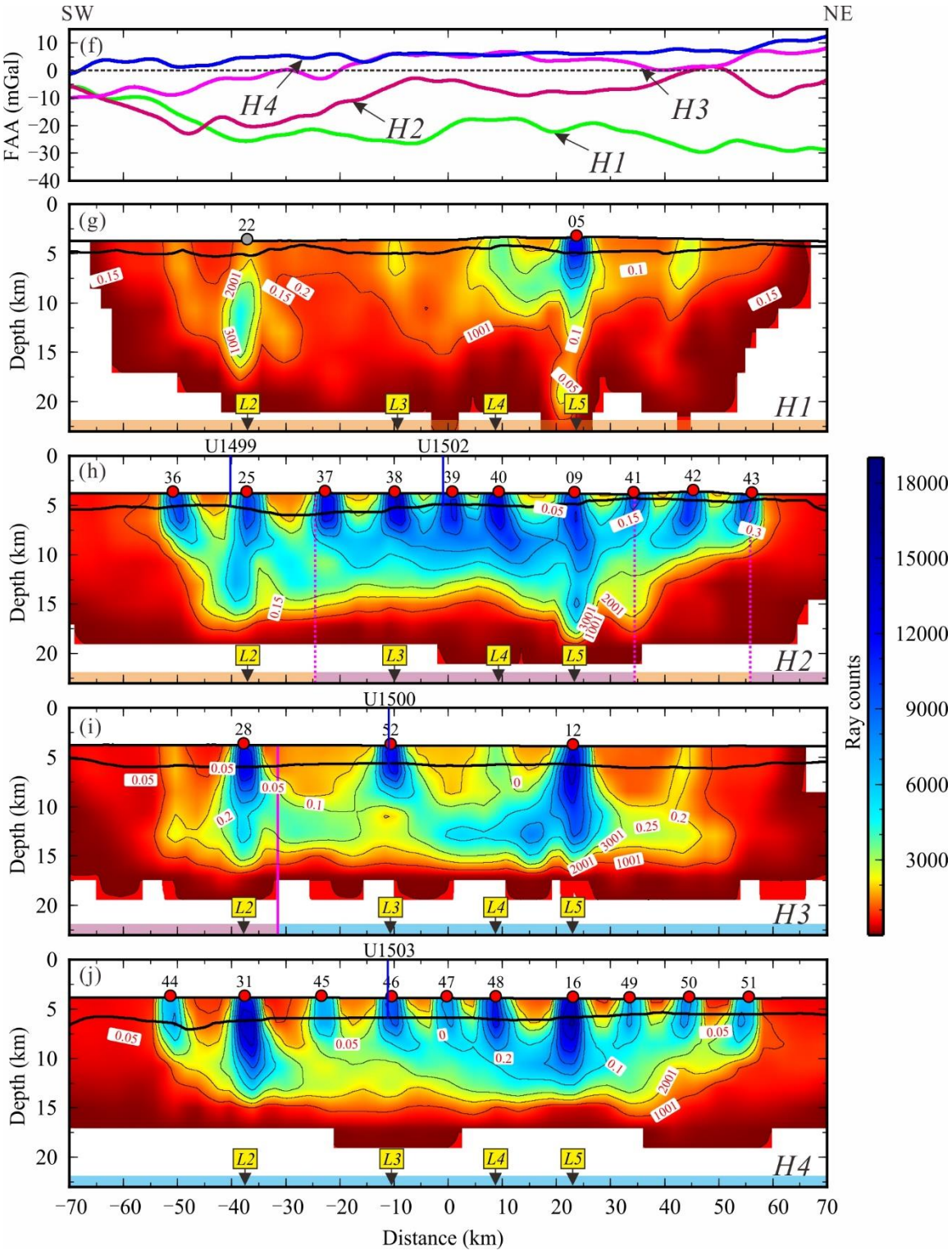

Figure S3 (Continuous).

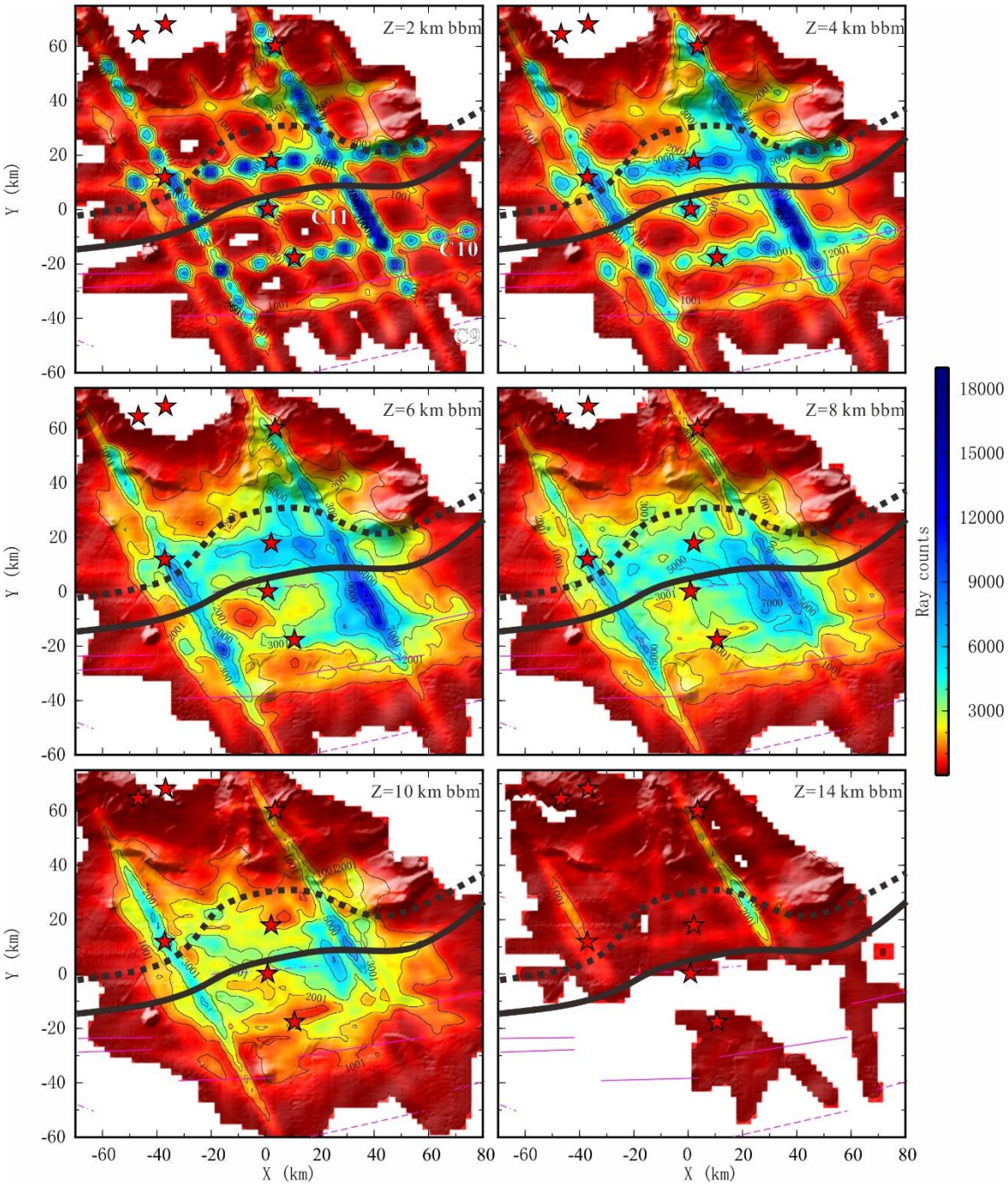

Figure S4. Horizontal slices of the 3D raytracing count model at different depths below TOB (bbm). The other symbols are same as Figure 6.

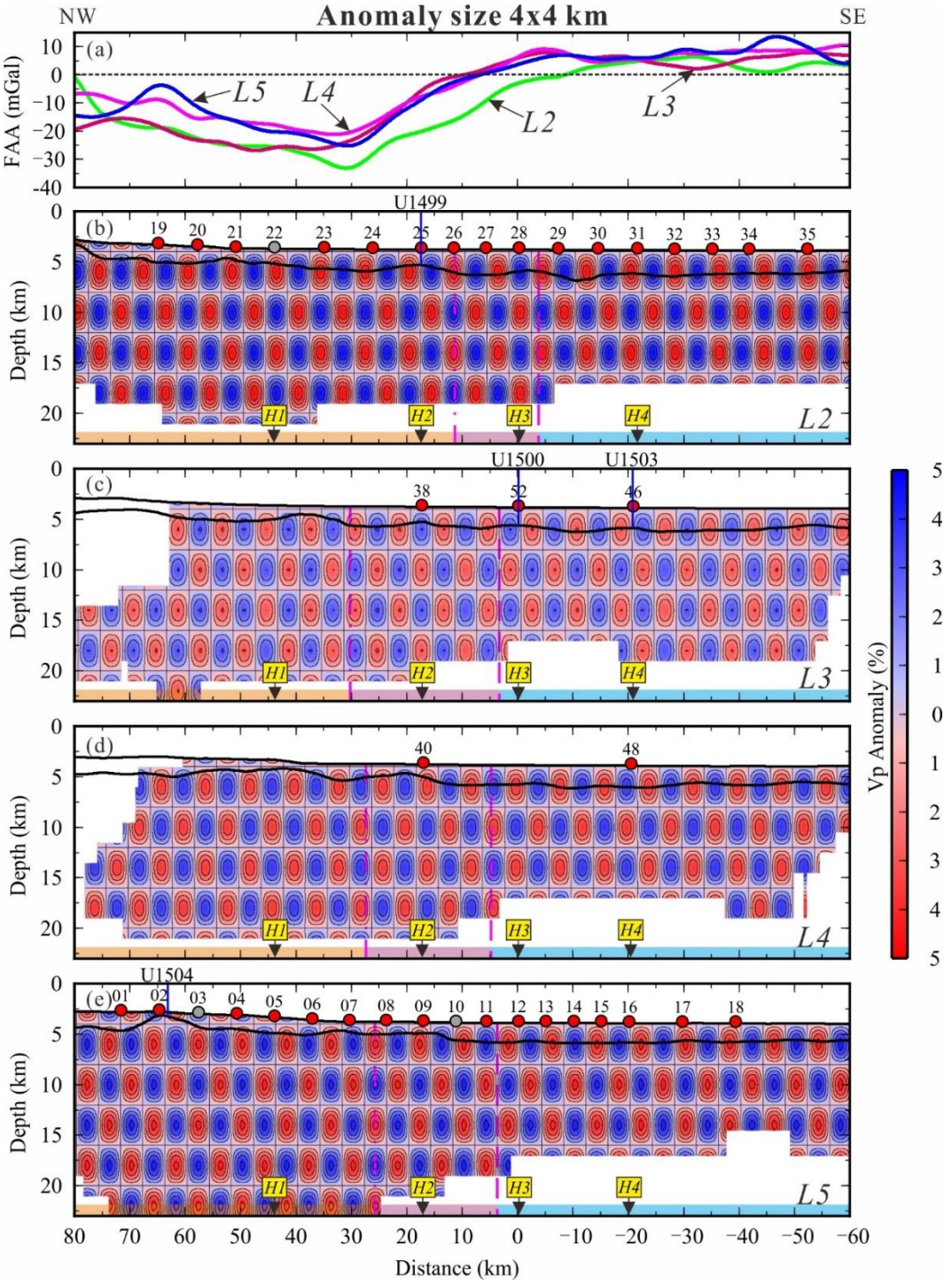

Figure S5. Vertical slices crosscutting the 3D models with true checkerboard pattern of the 4x4 km (a-e), 10x10 km (a'-e') and 20x20 km (a''-e'') anomaly size. The other symbols are same as Figure 5.

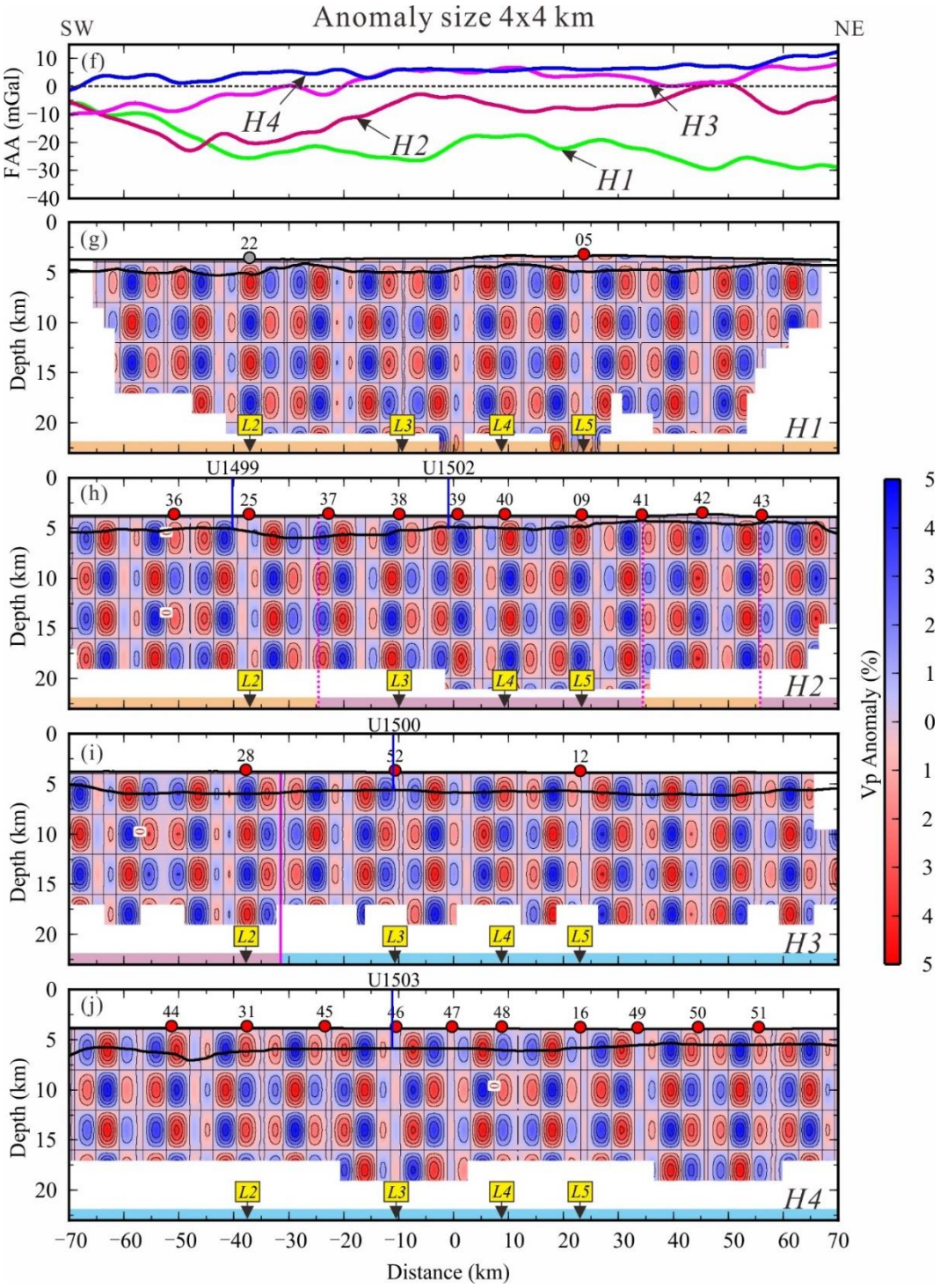

Figure S5 (Continuous).

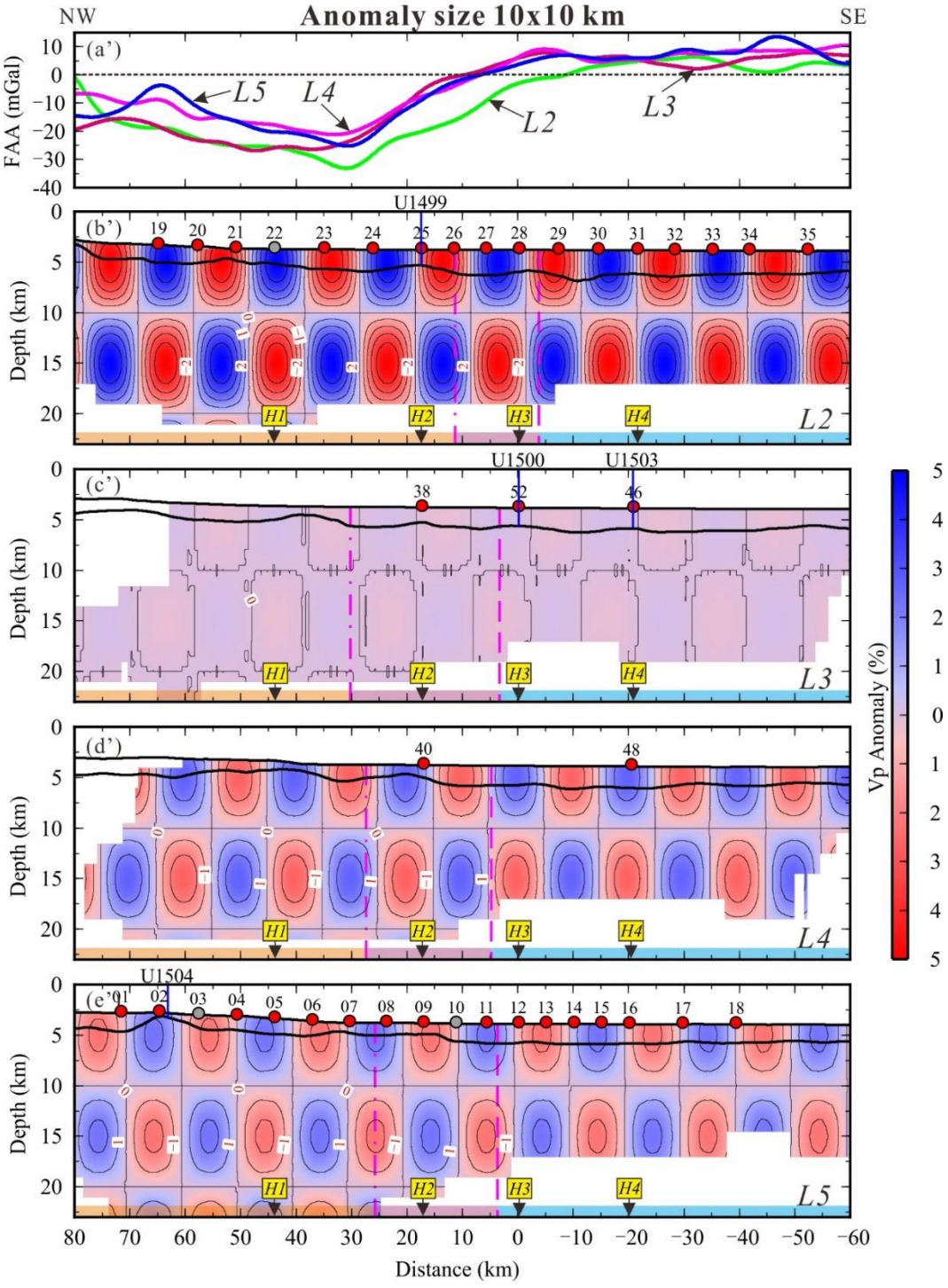

Figure S5 (Continuous).

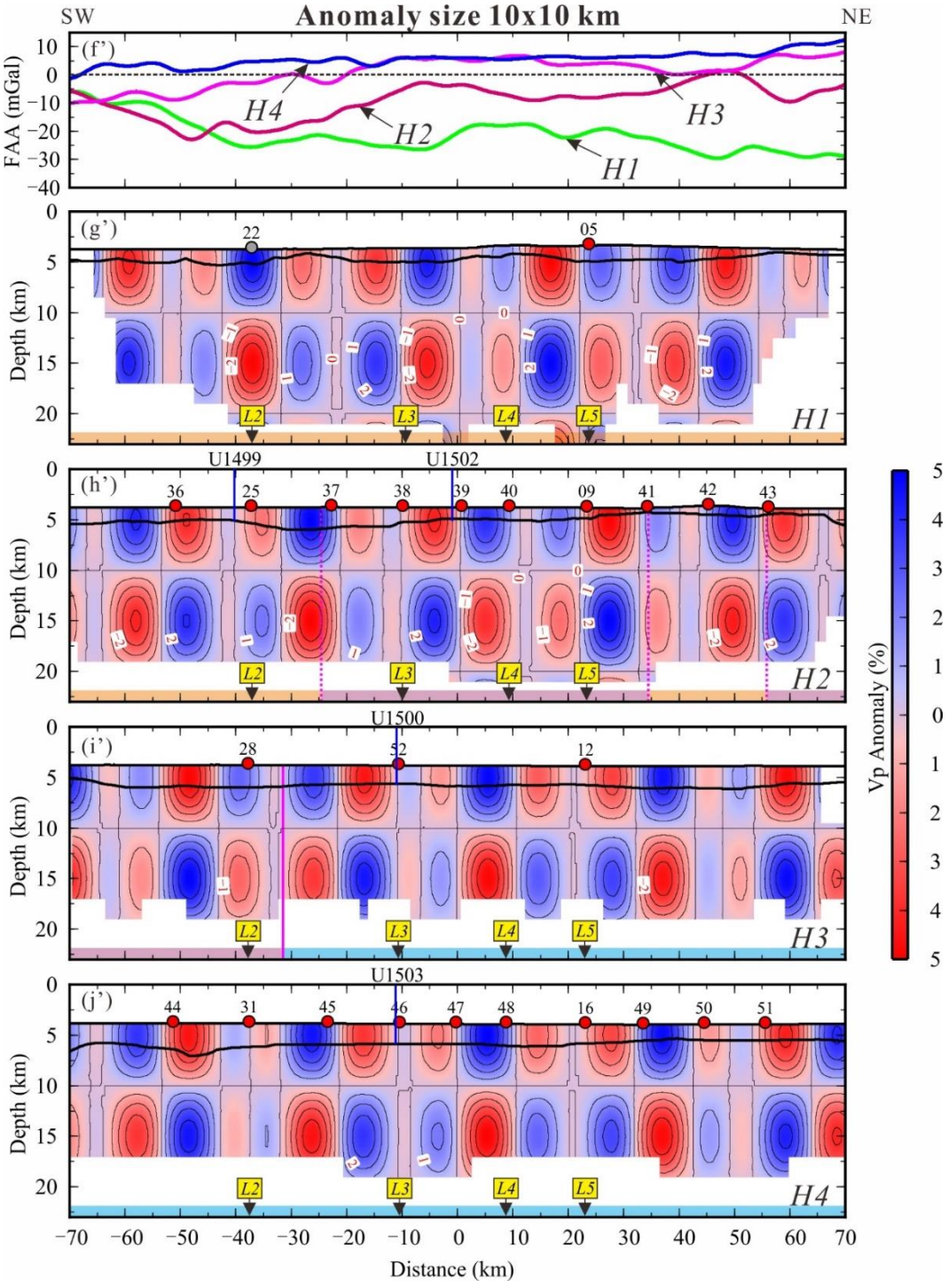

Figure S5 (Continuous).

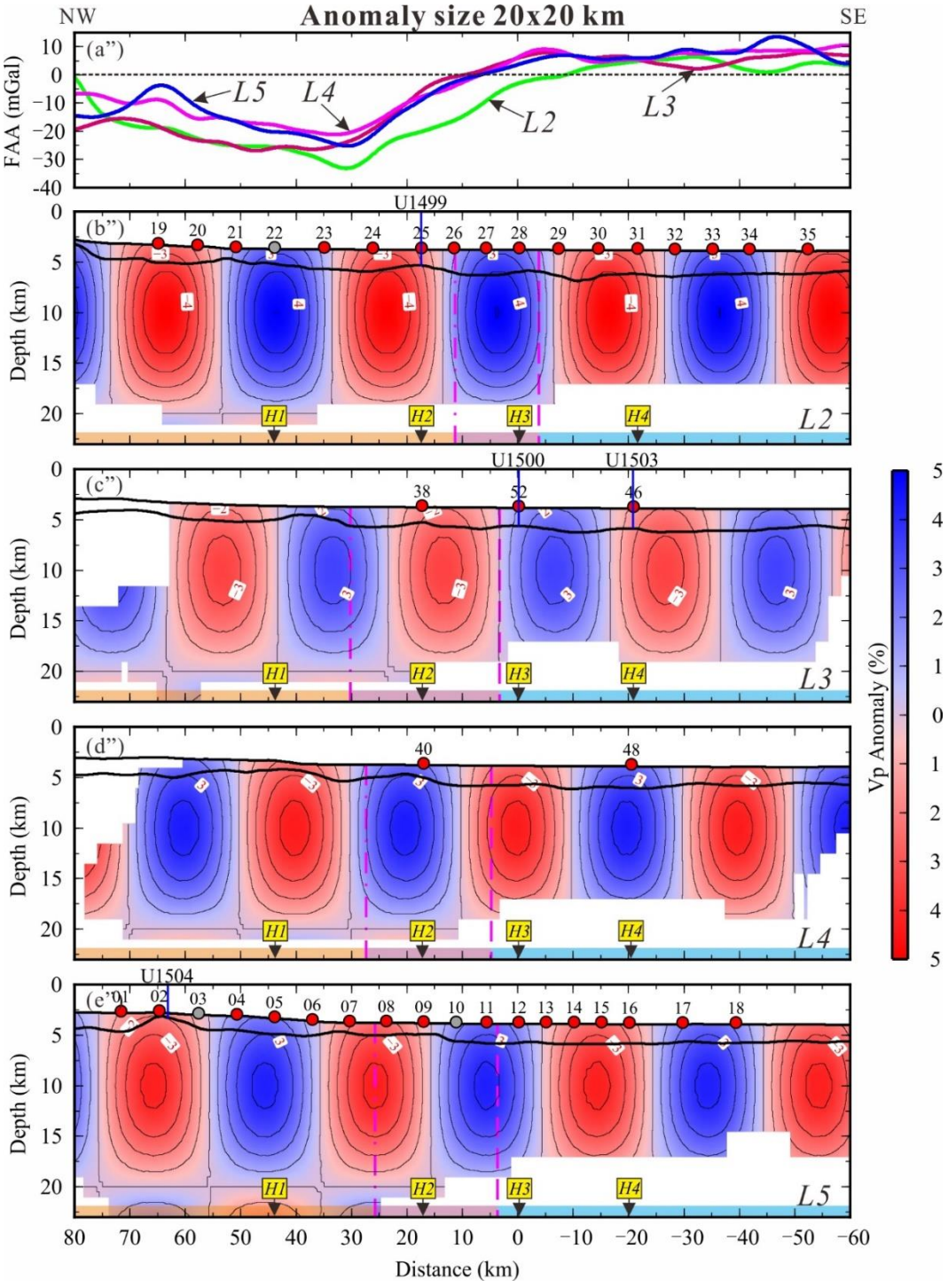

Figure S5 (Continuous).

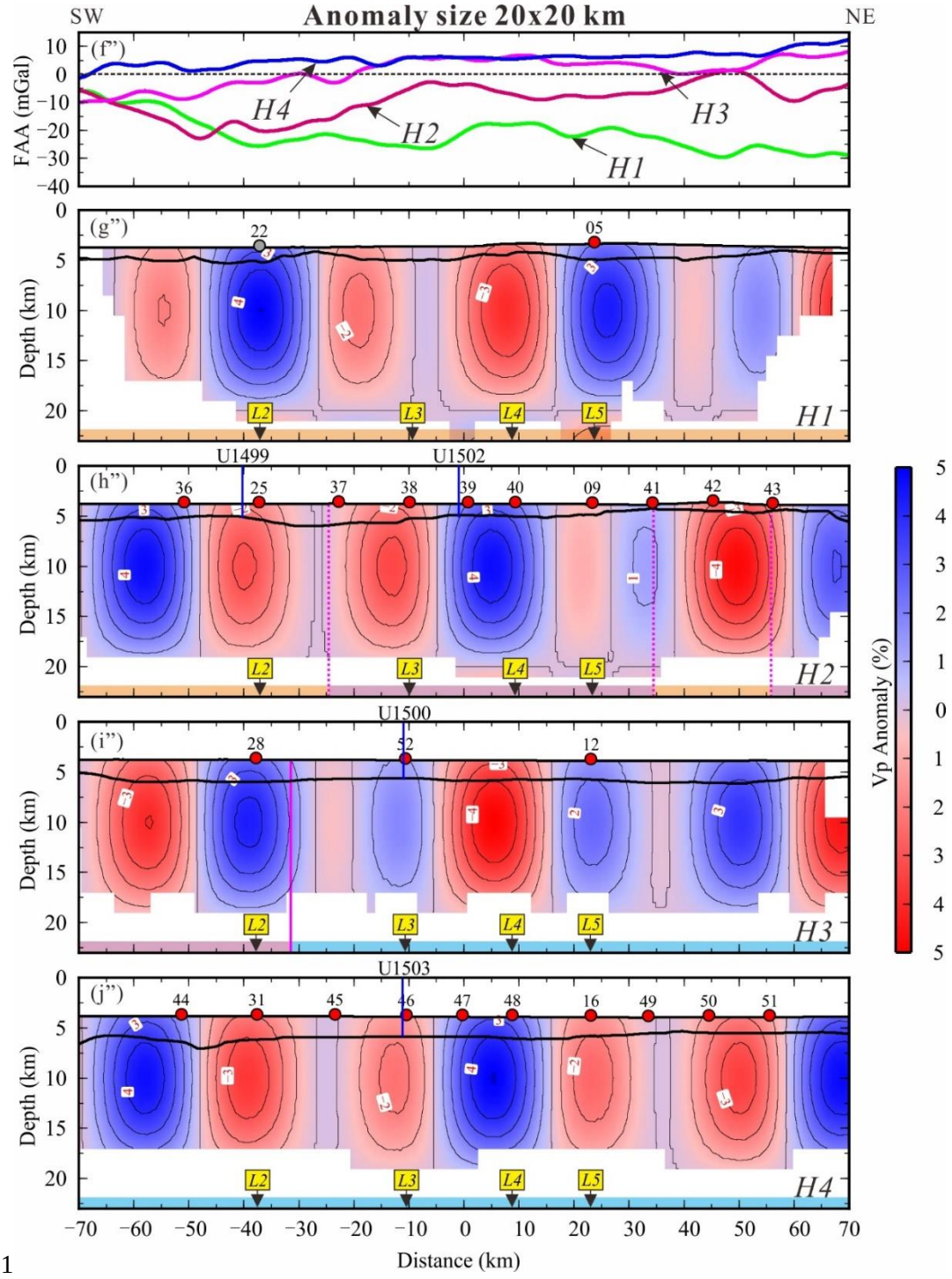

1

Figure S5 (Continuous).

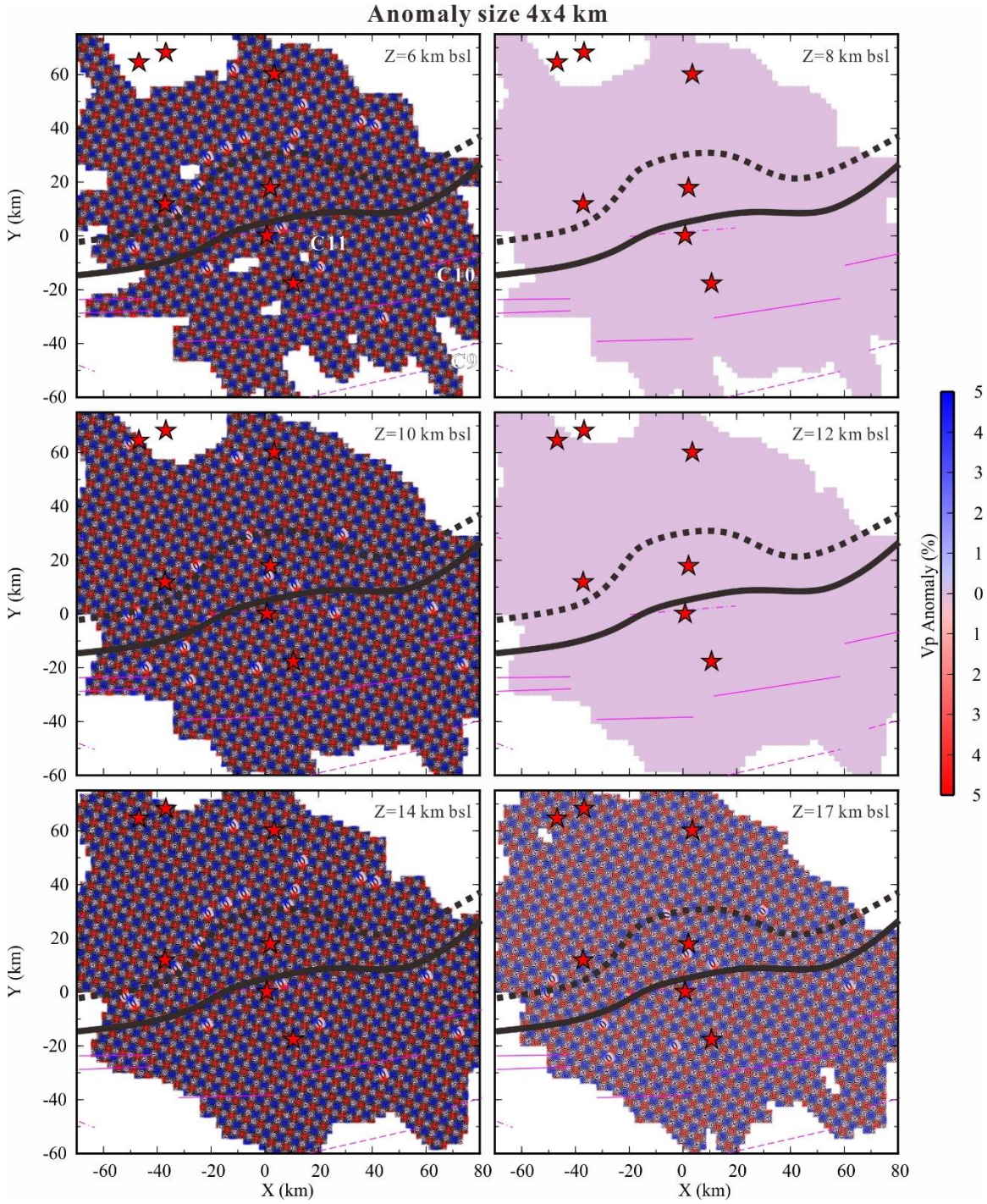

Figure S6. Horizontal slices of the 3D models with true checkerboard pattern of the 4x4 km, 10x10 km and 20x20 km anomaly size at different depths below sea level (bsl). The other symbols are same as Figure 6.

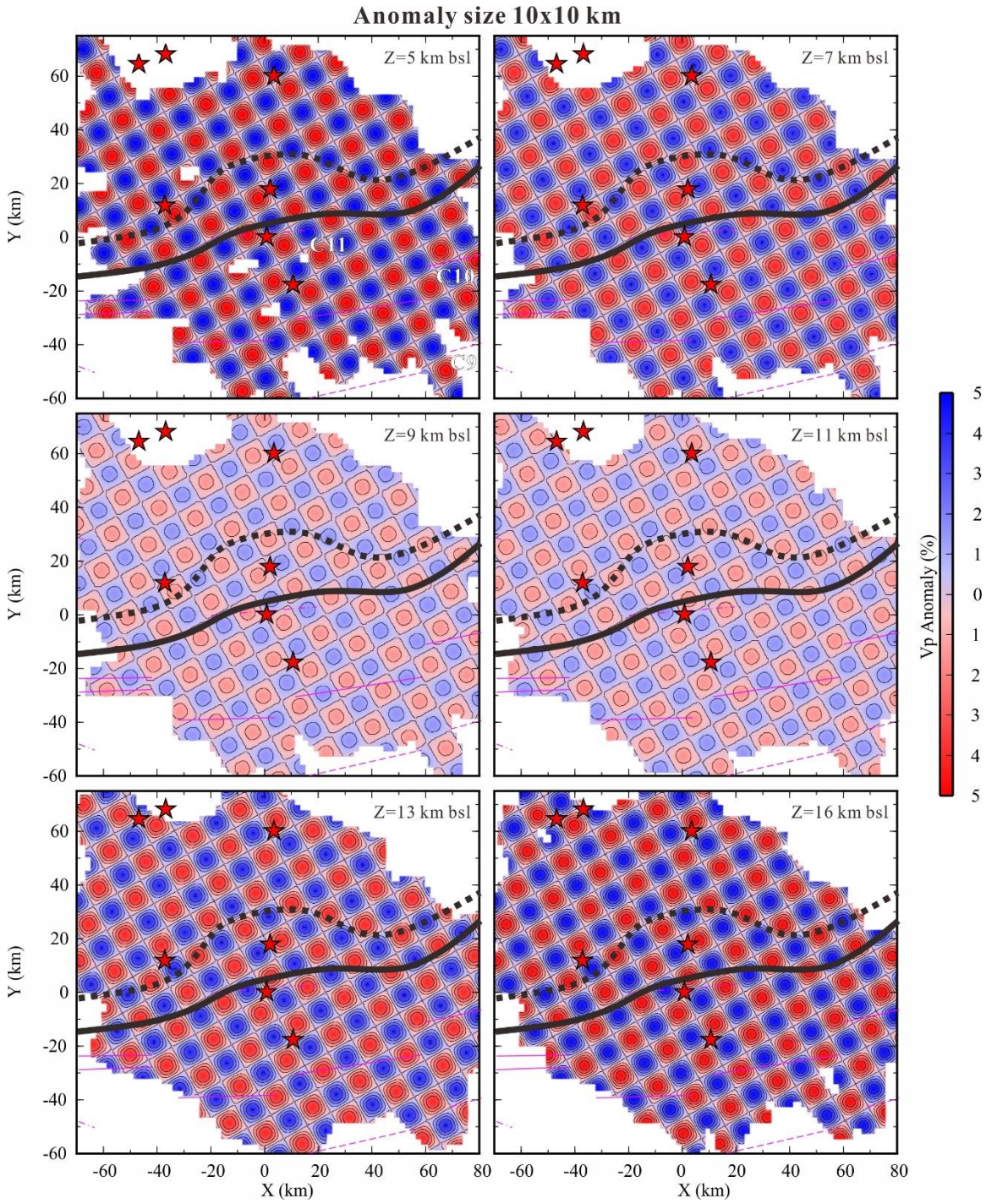

Figure S6 (Continuous).

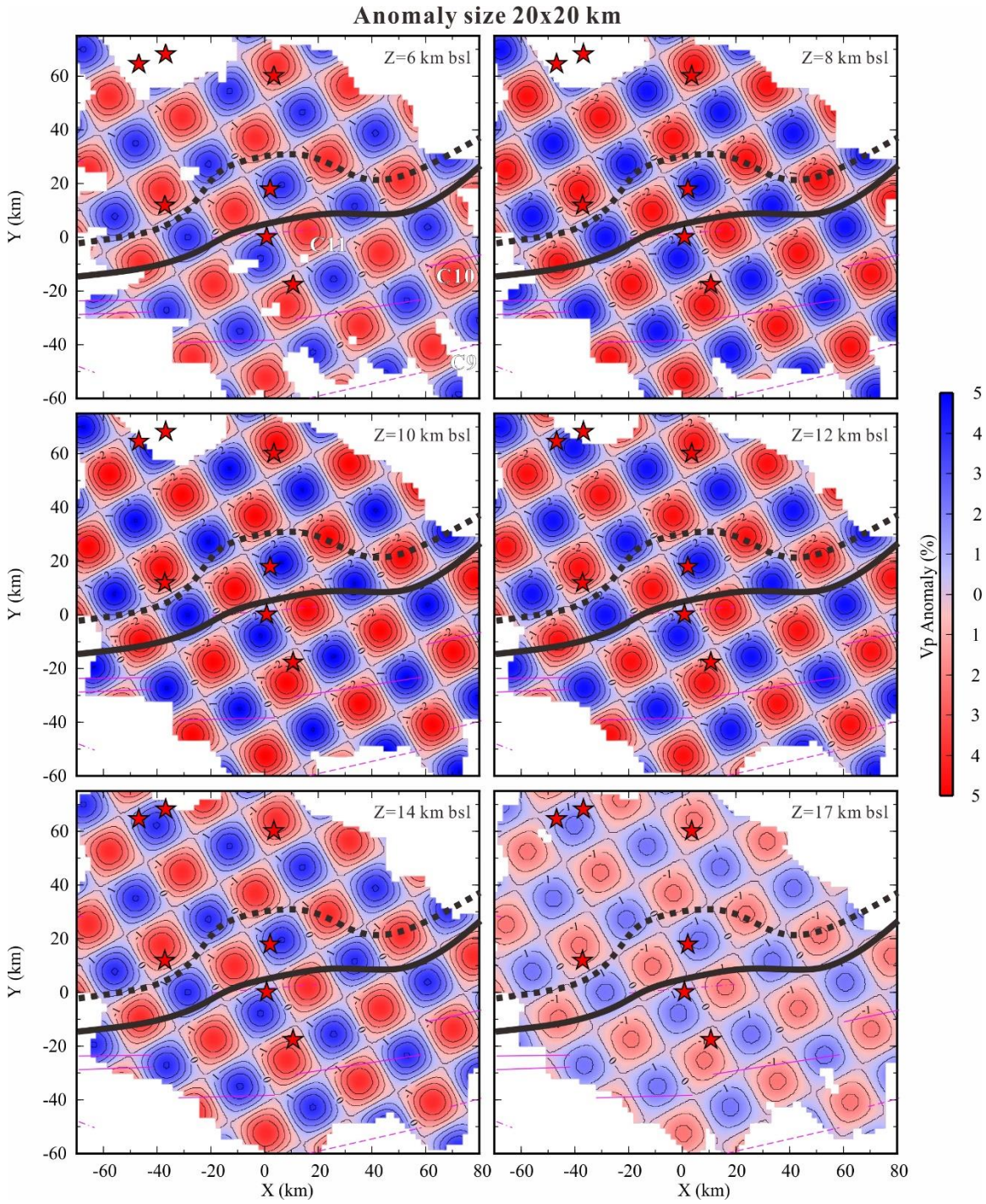

Figure S6 (Continuous).

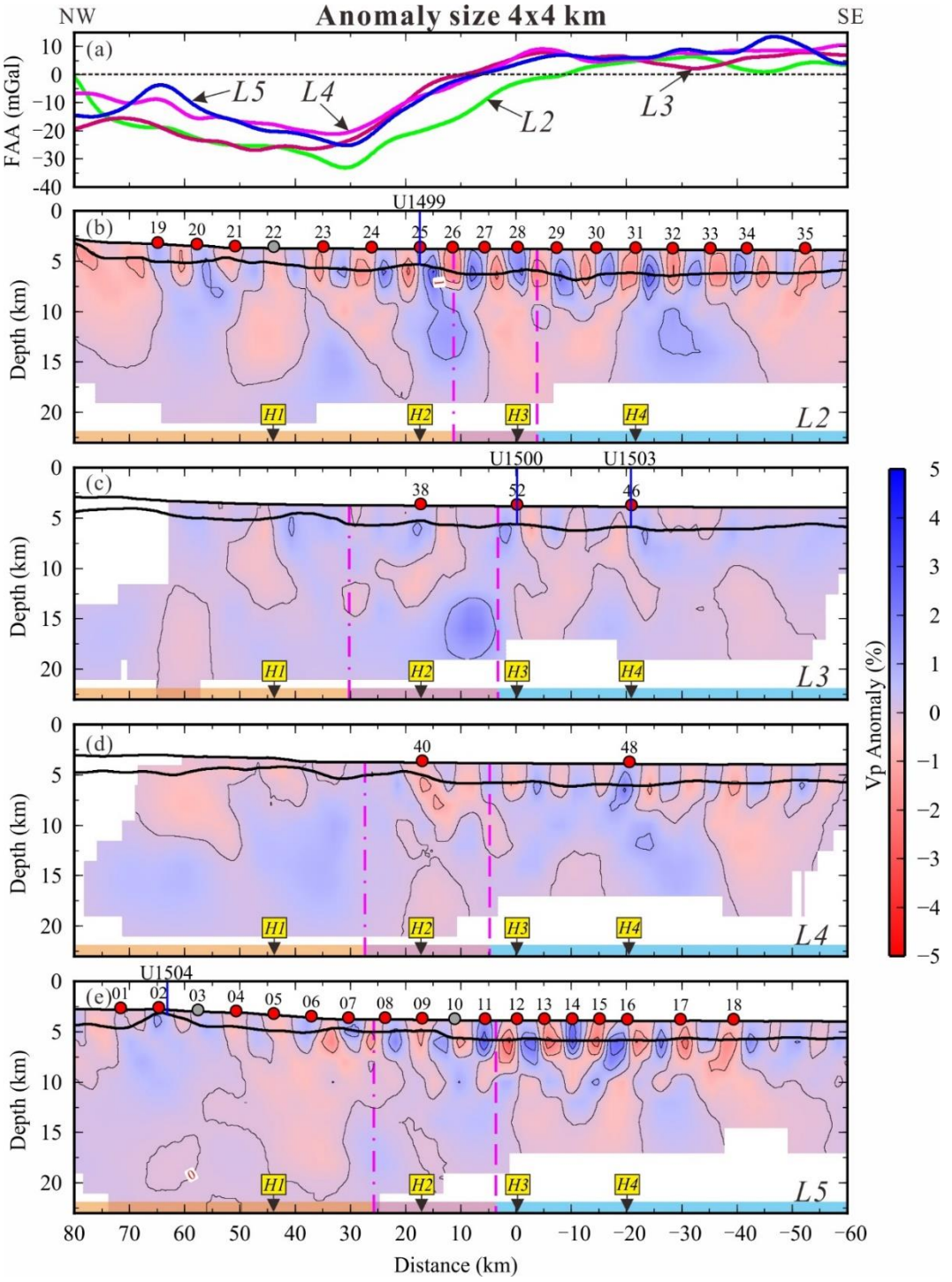

Figure S7. Vertical slices crosscutting the 3D models with retrieved checkerboard pattern of the 4x4 km (a-e), 10x10 km (a'-e') and 20x20 km (a''-e'') anomaly size. The other symbols are same as Figure 5.

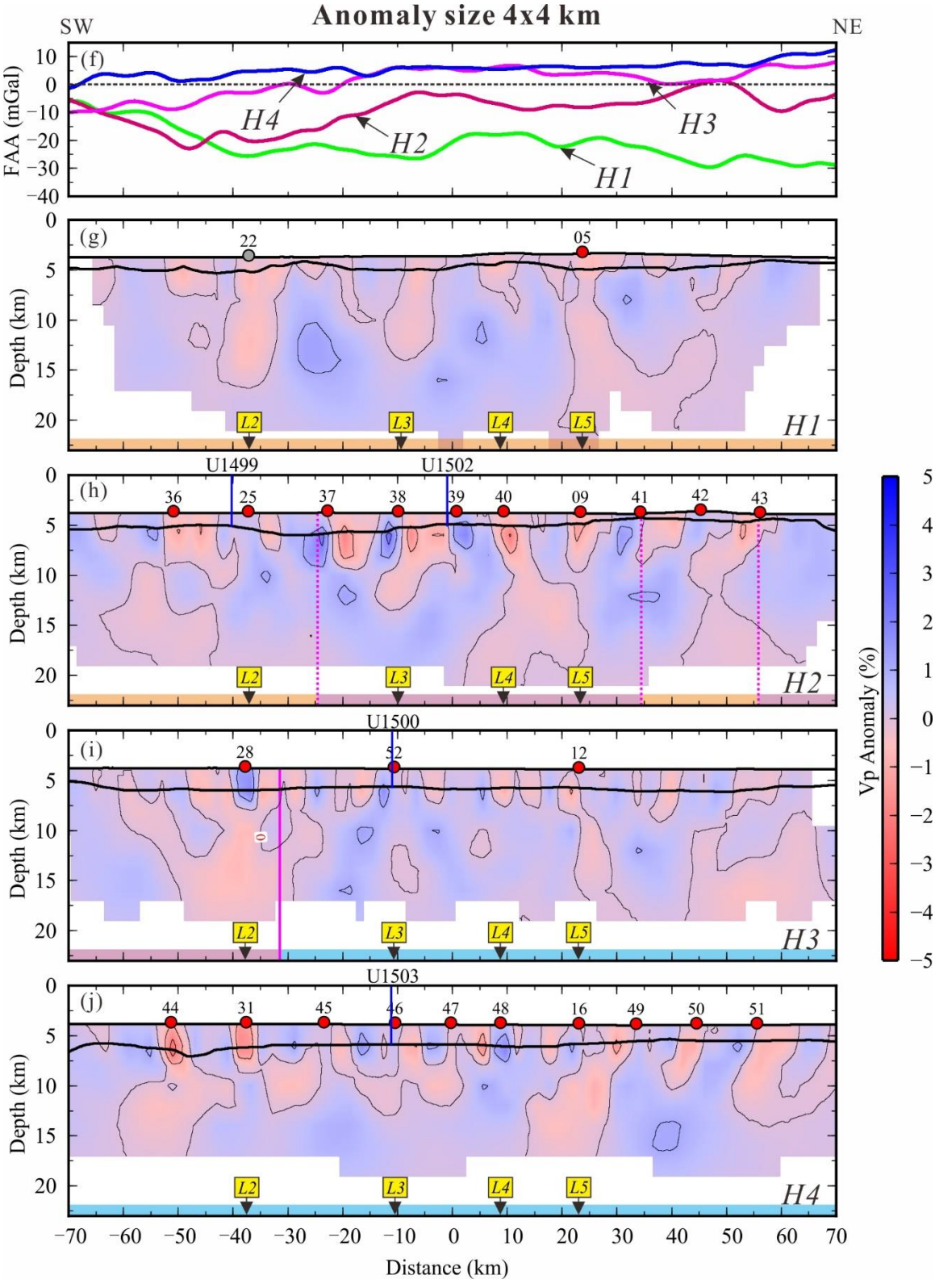

Figure S7 (Continuous).

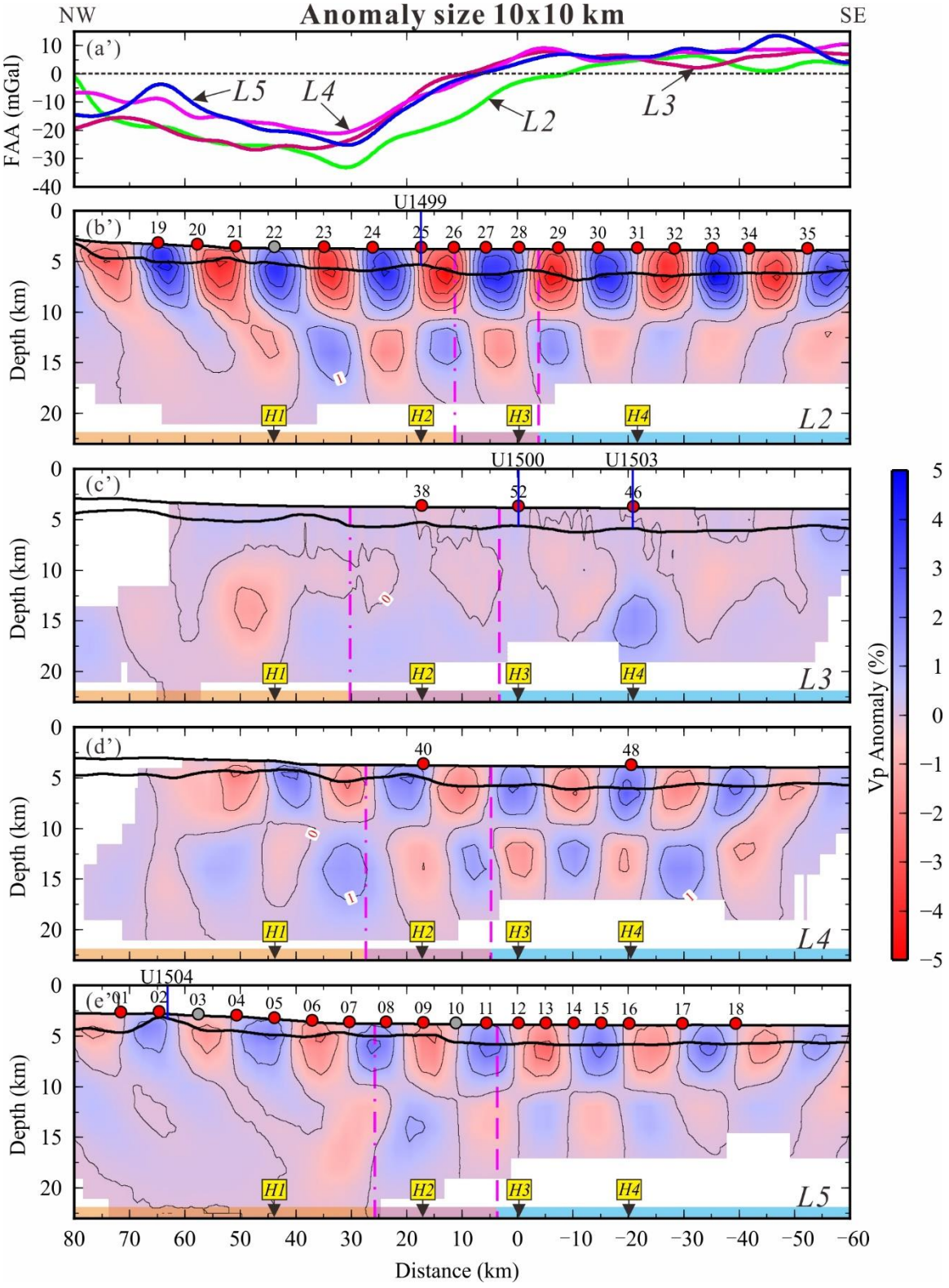

Figure S7 (Continuous).

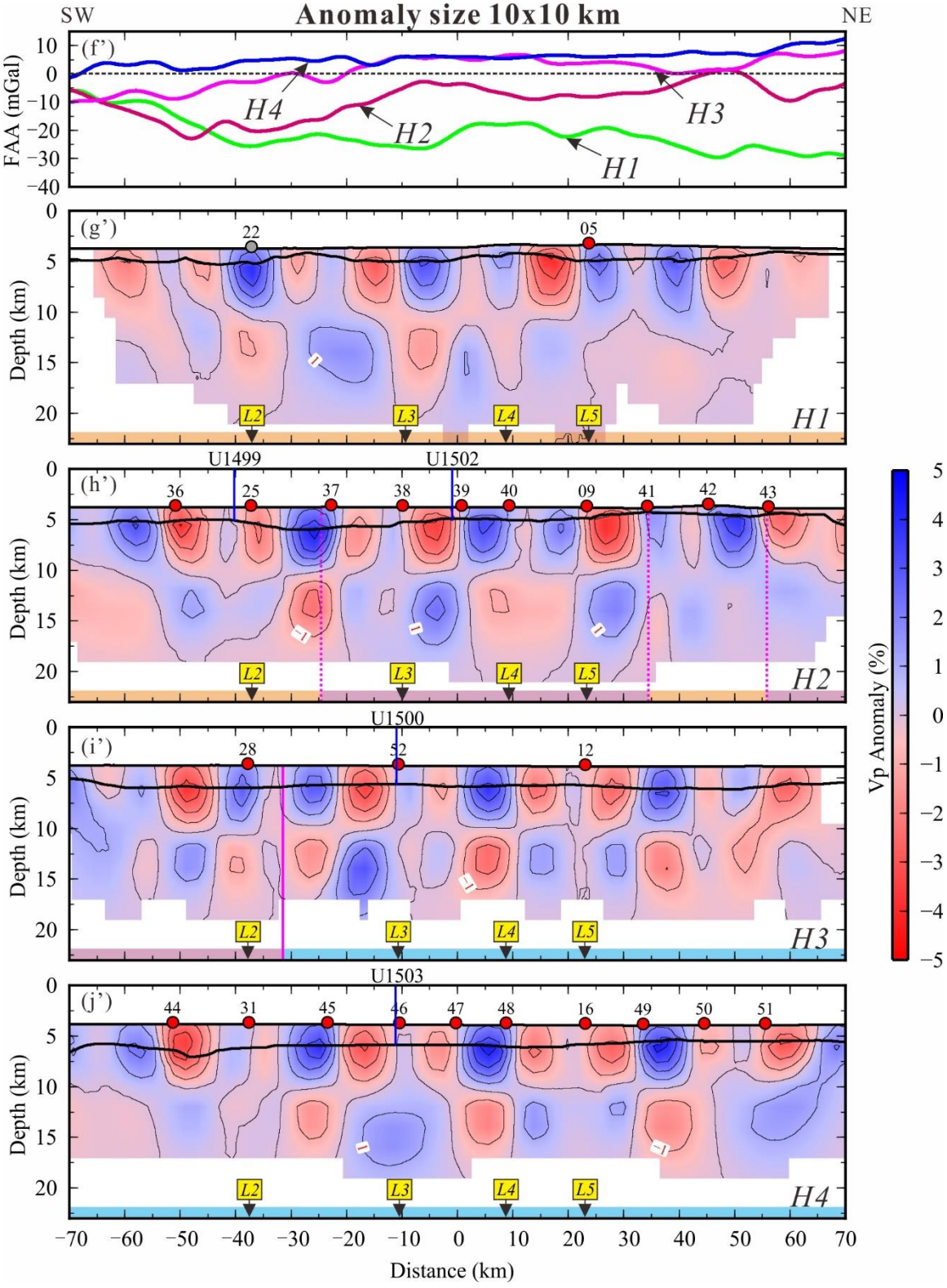

Figure S7 (Continuous).

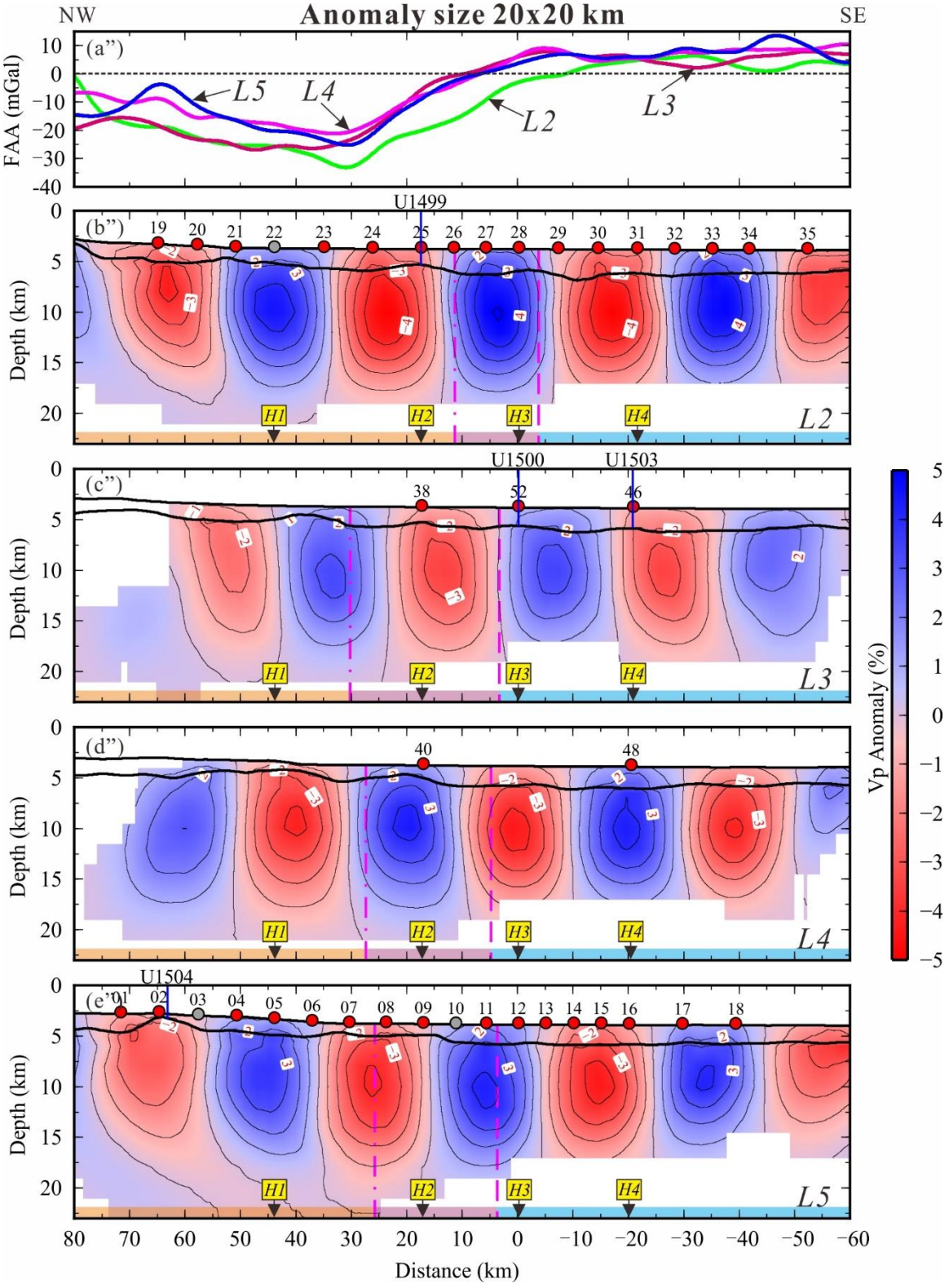

Figure S7 (Continuous).

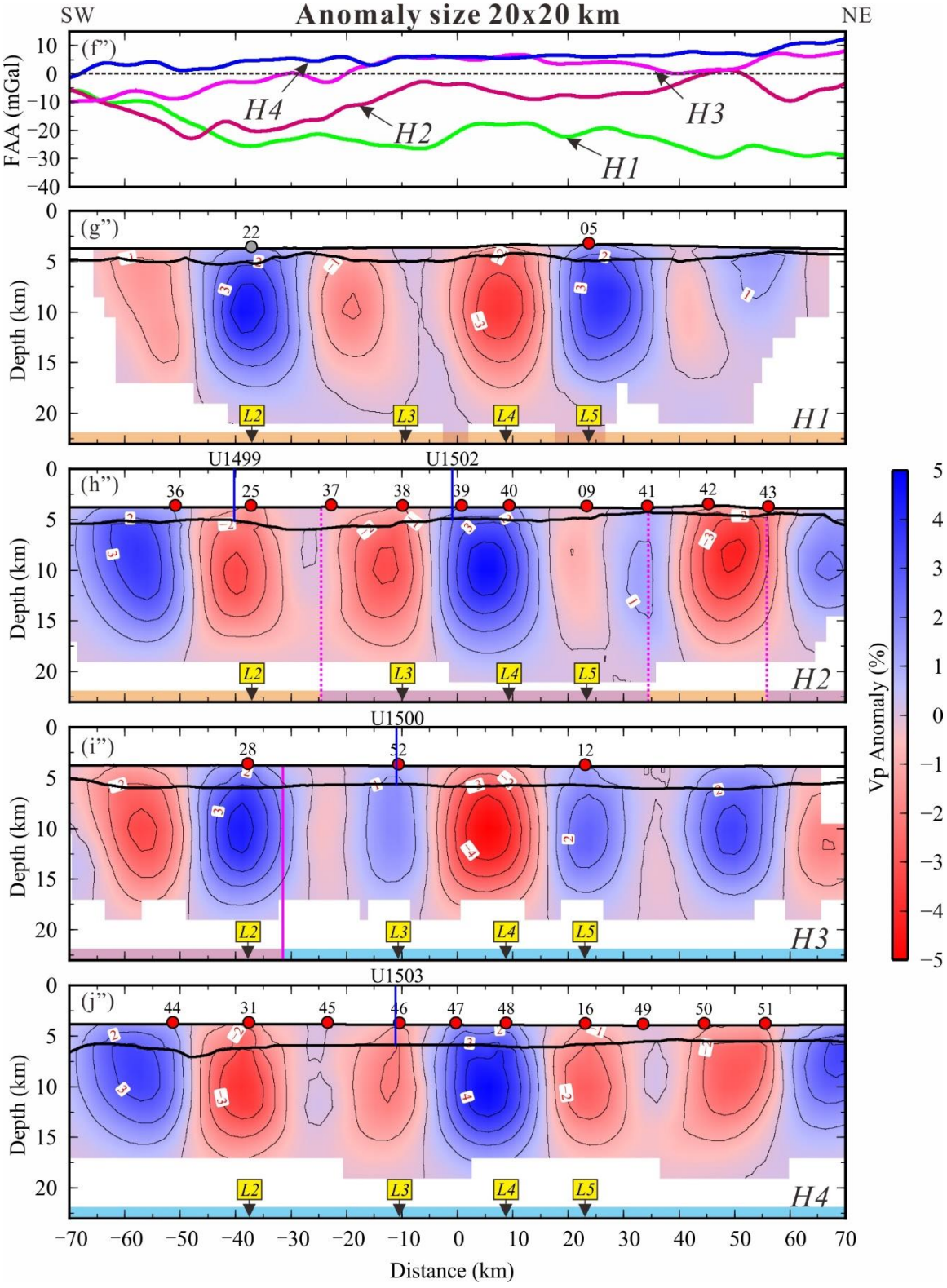

Figure S7 (Continuous).

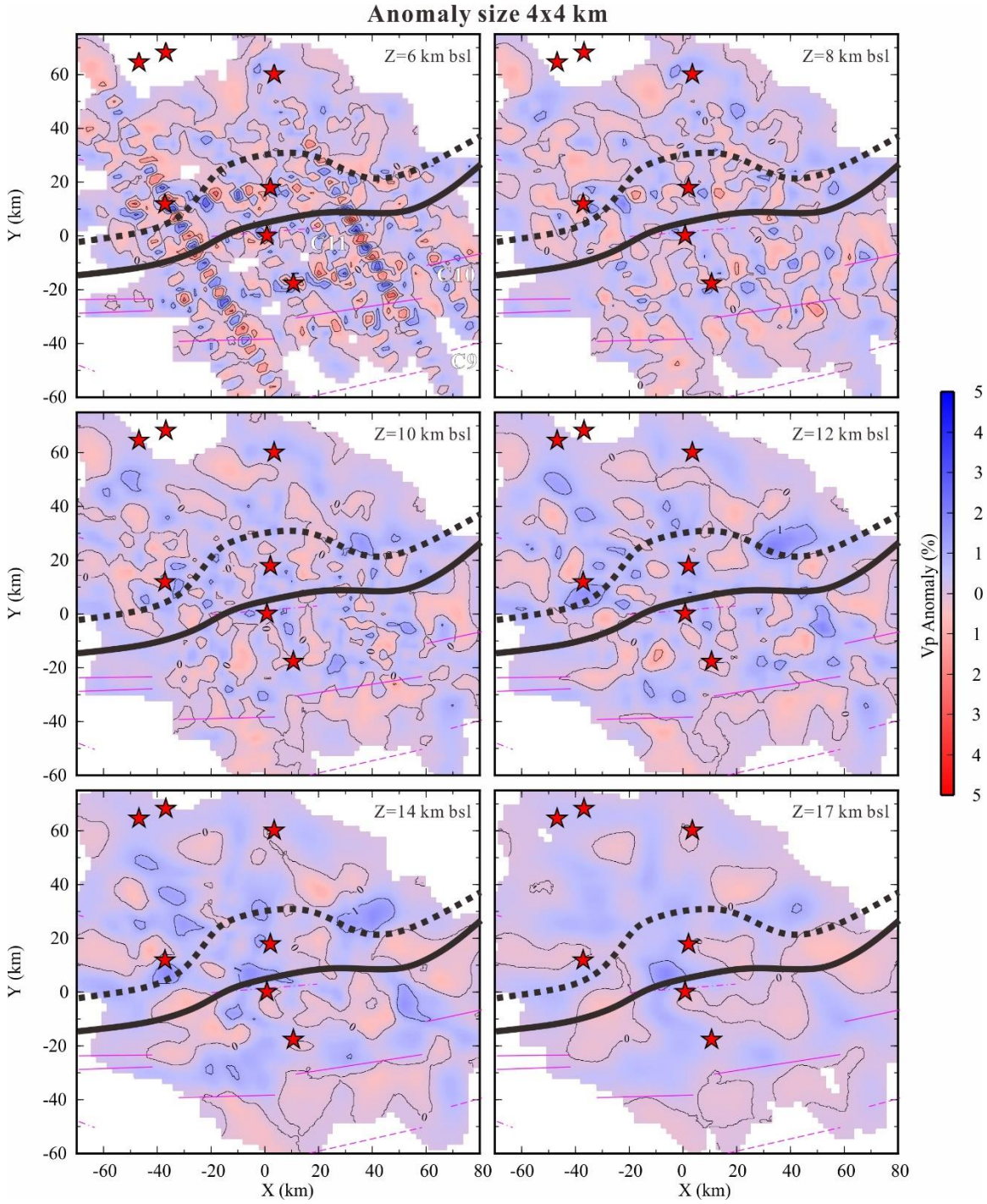

Figure S8. Horizontal slices of the 3D models with retrieved checkerboard pattern of the 4x4 km, 10x10 km and 20x20 km anomaly size at different depths below sea level (bsl). The other symbols are same as Figure 6.

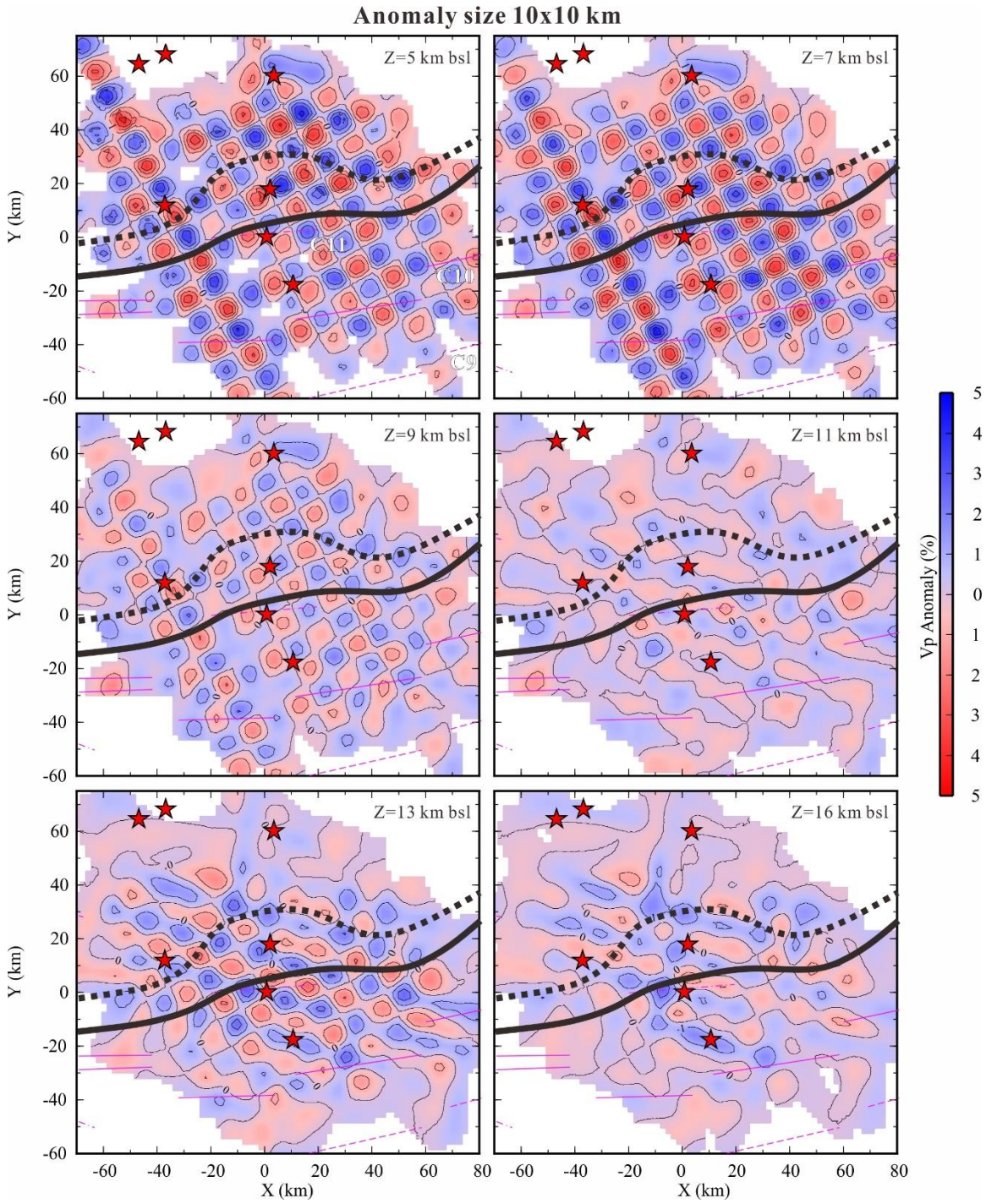

Figure S8 (Continuous).

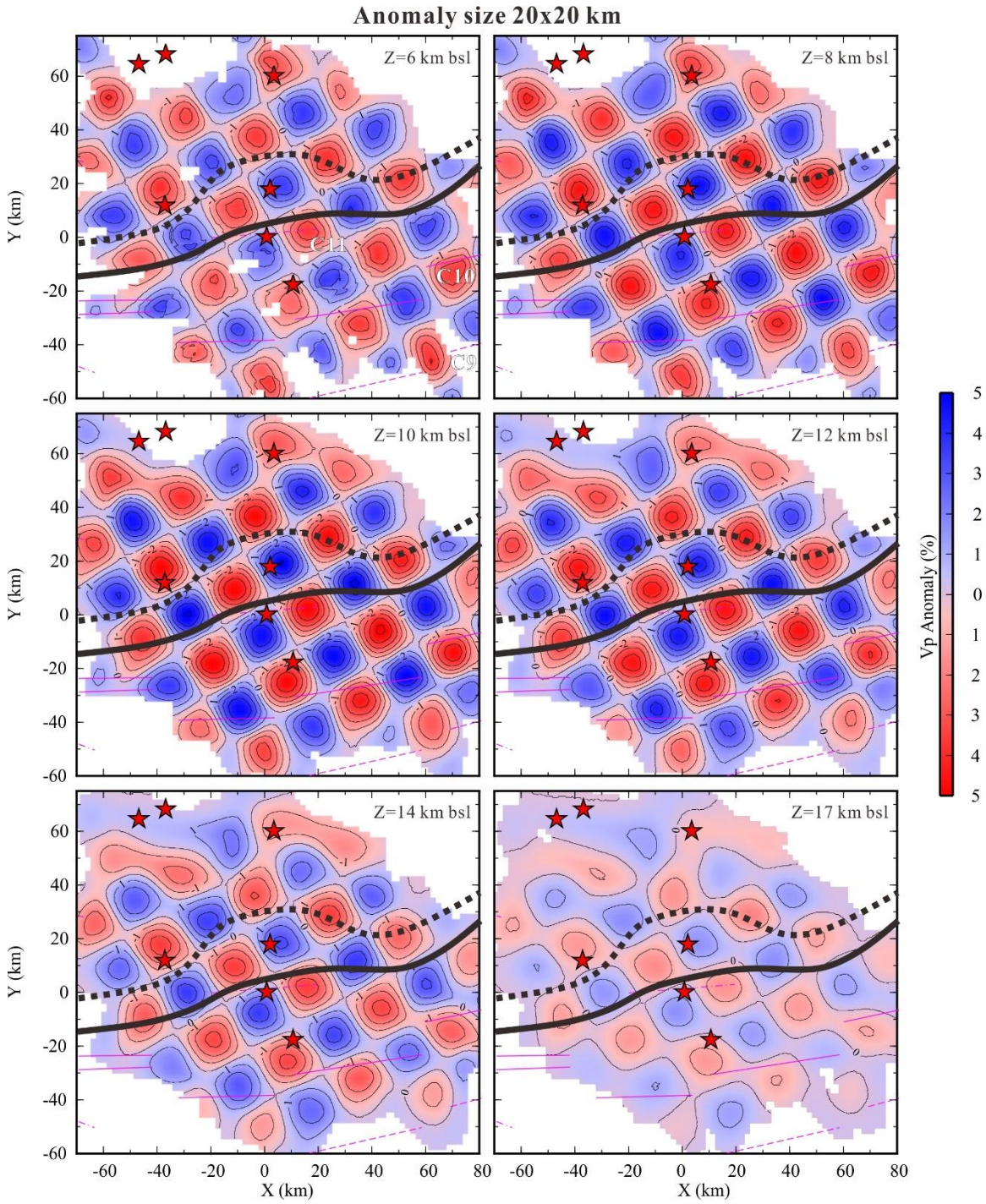

Figure S8 (Continuous).

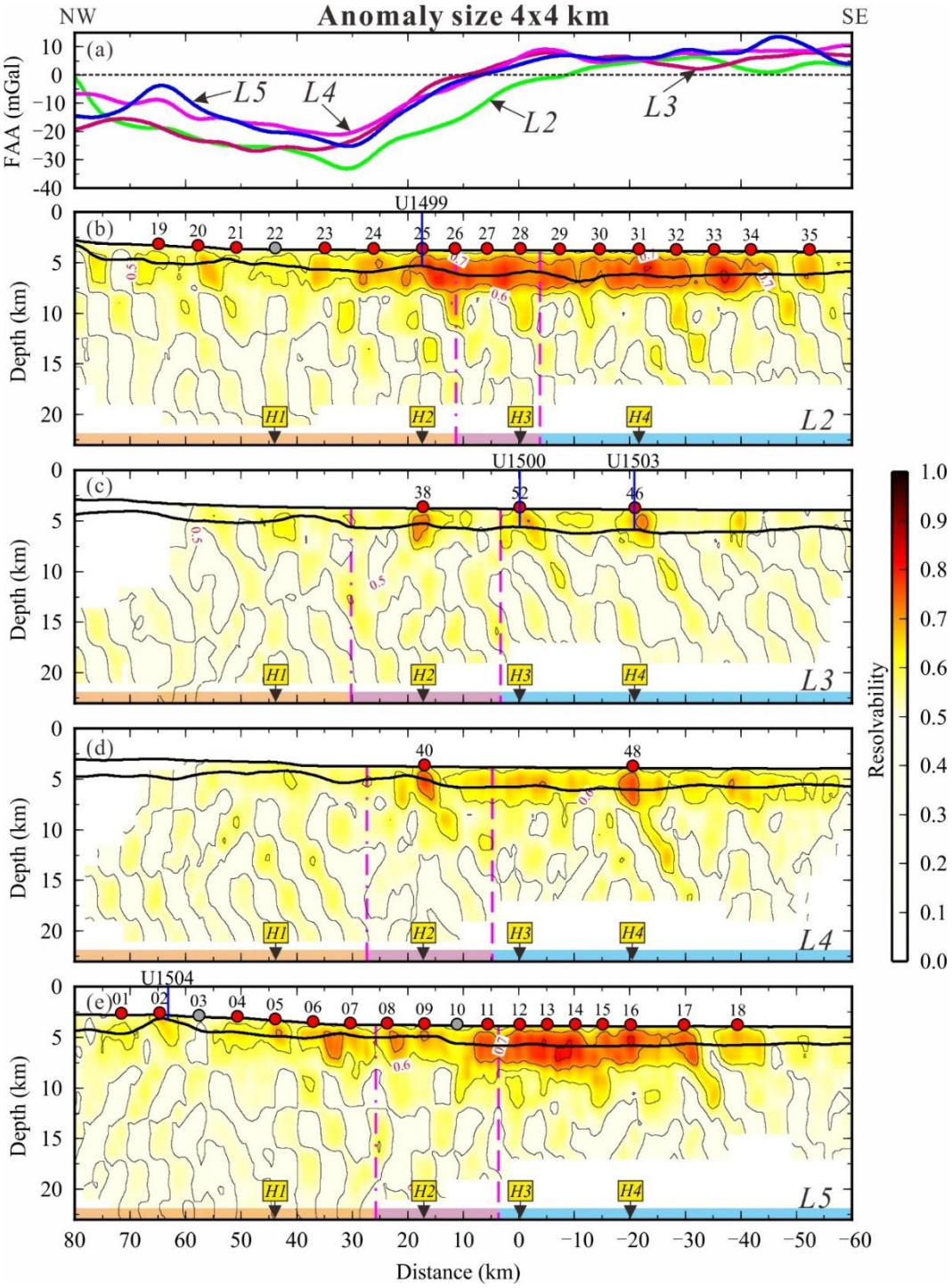

Figure S9. Vertical slices crosscutting the 3D resolvability models with retrieved checkerboard pattern of the 4x4 km (a-e), 10x10 km (a'-e') and 20x20 km (a''-e'') anomaly size. The other symbols are same as Figure 5.

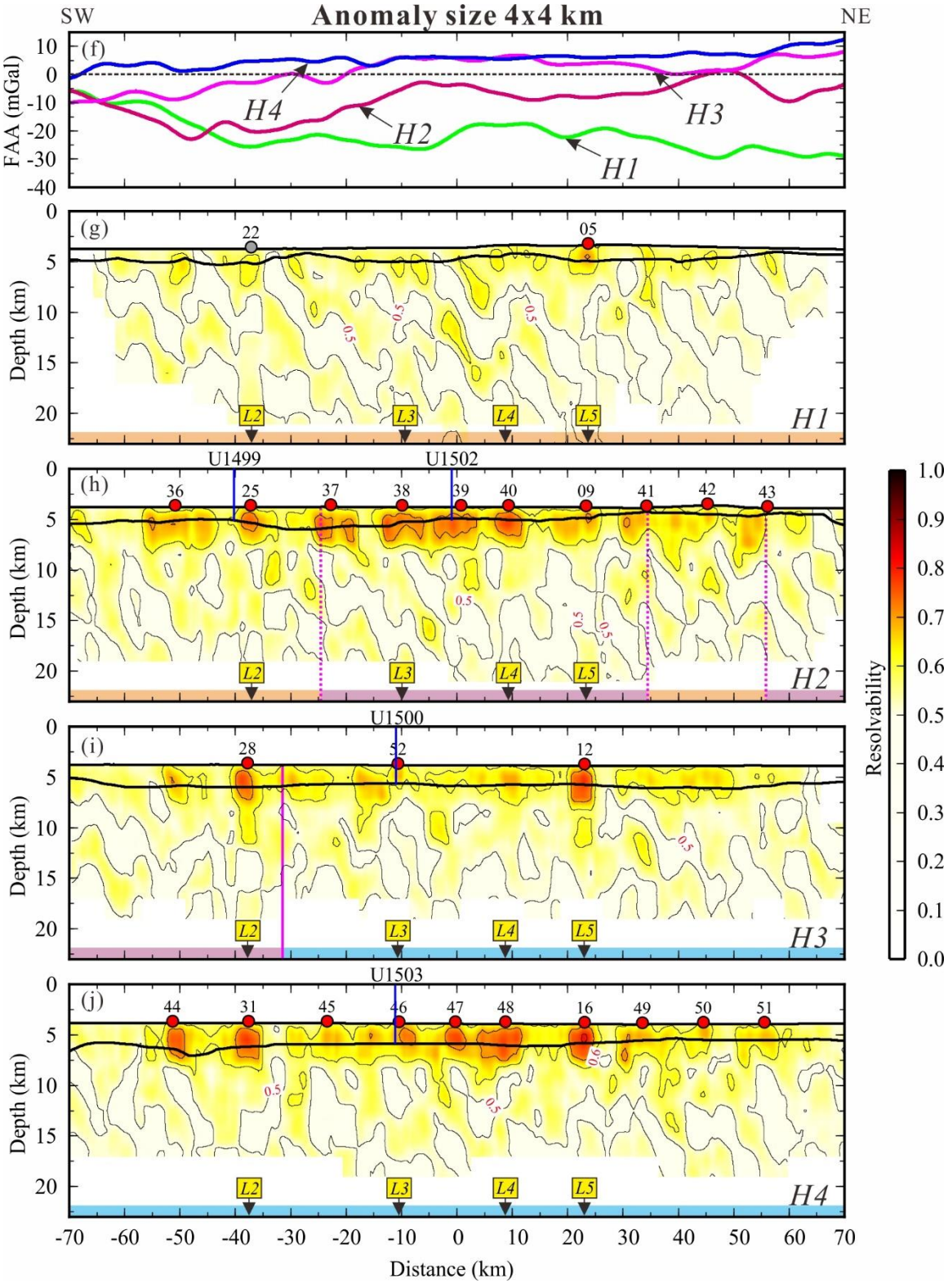

Figure S9 (Continuous).

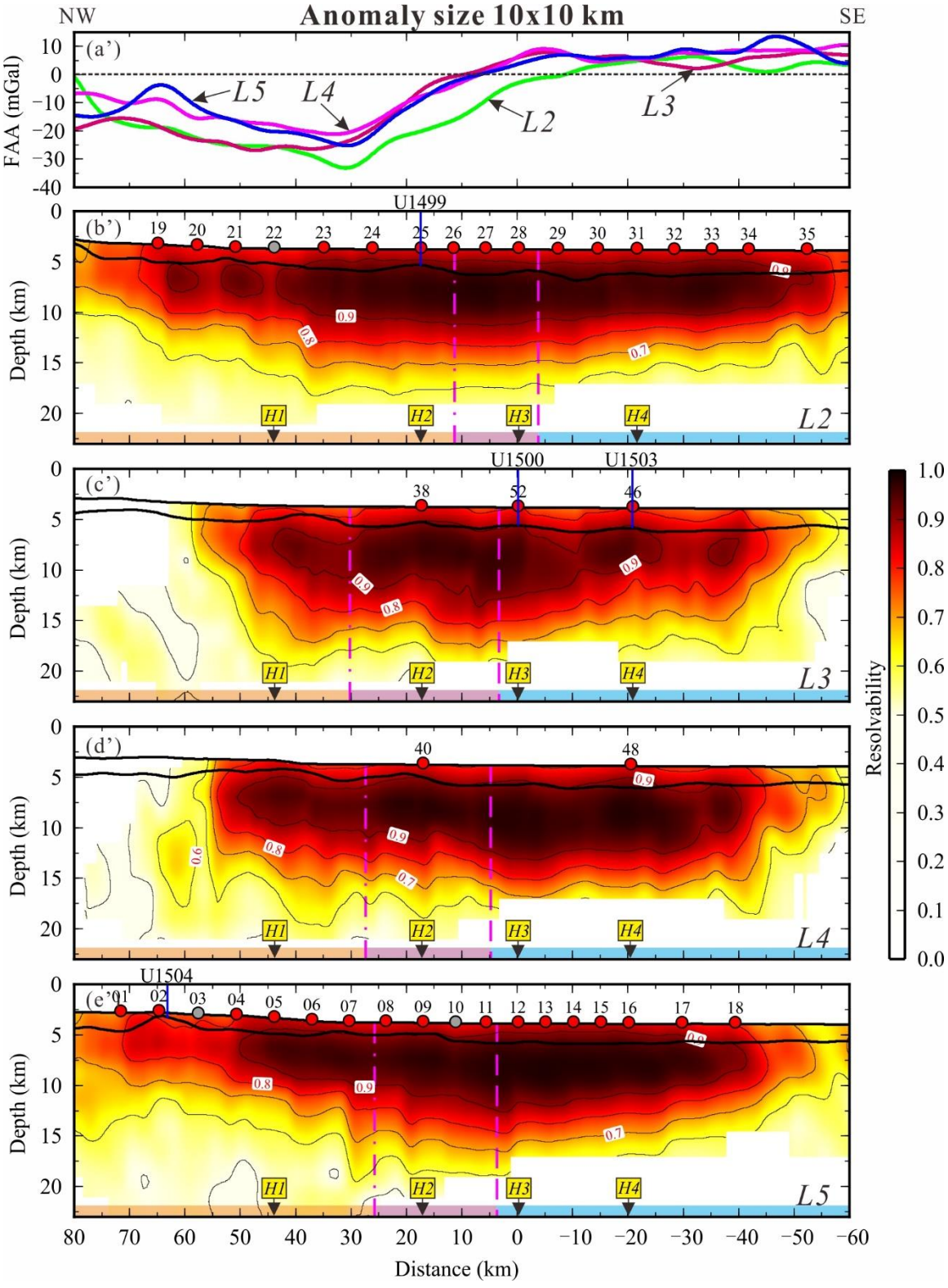

Figure S9 (Continuous).

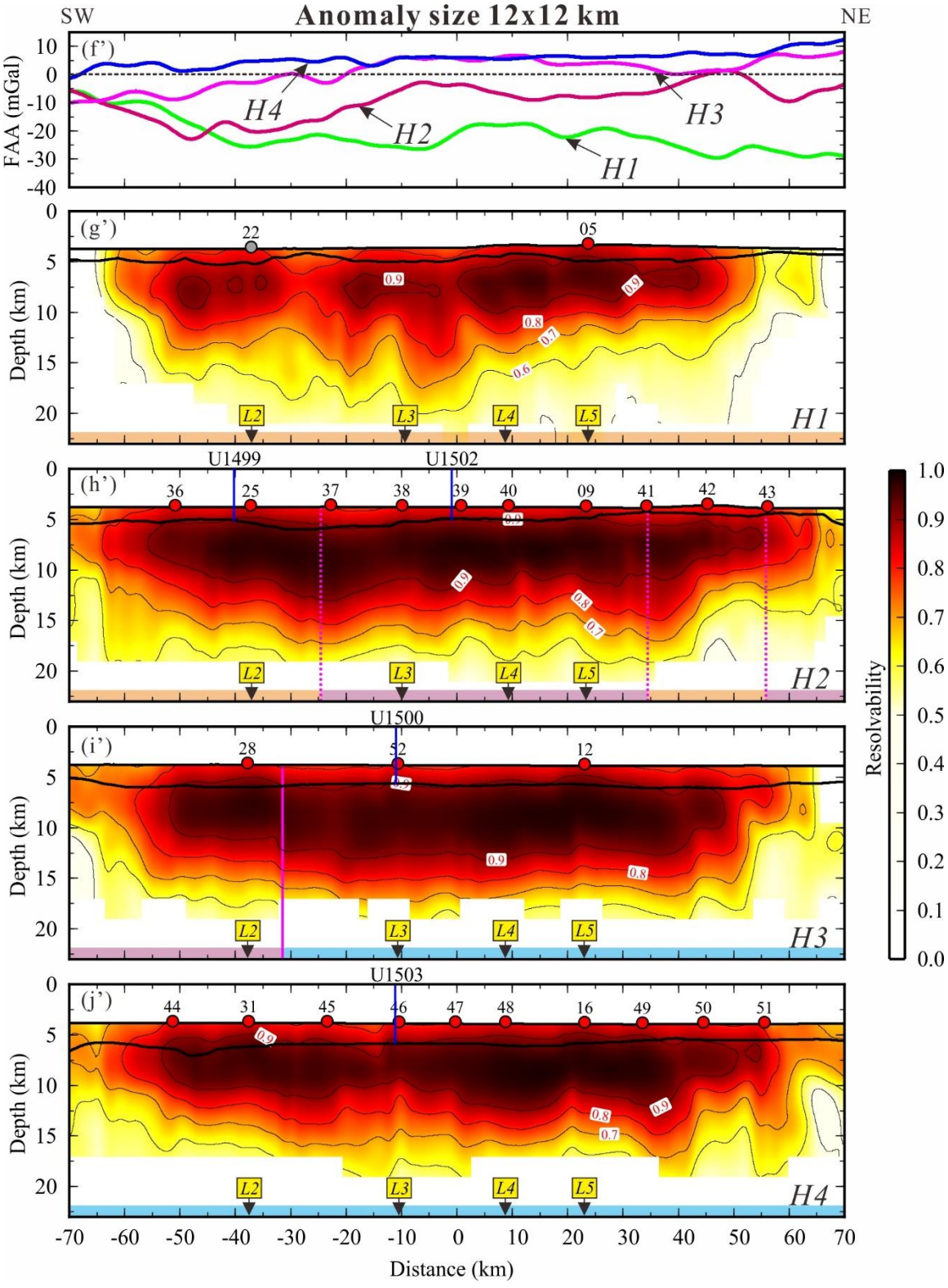

Figure S9 (Continuous).

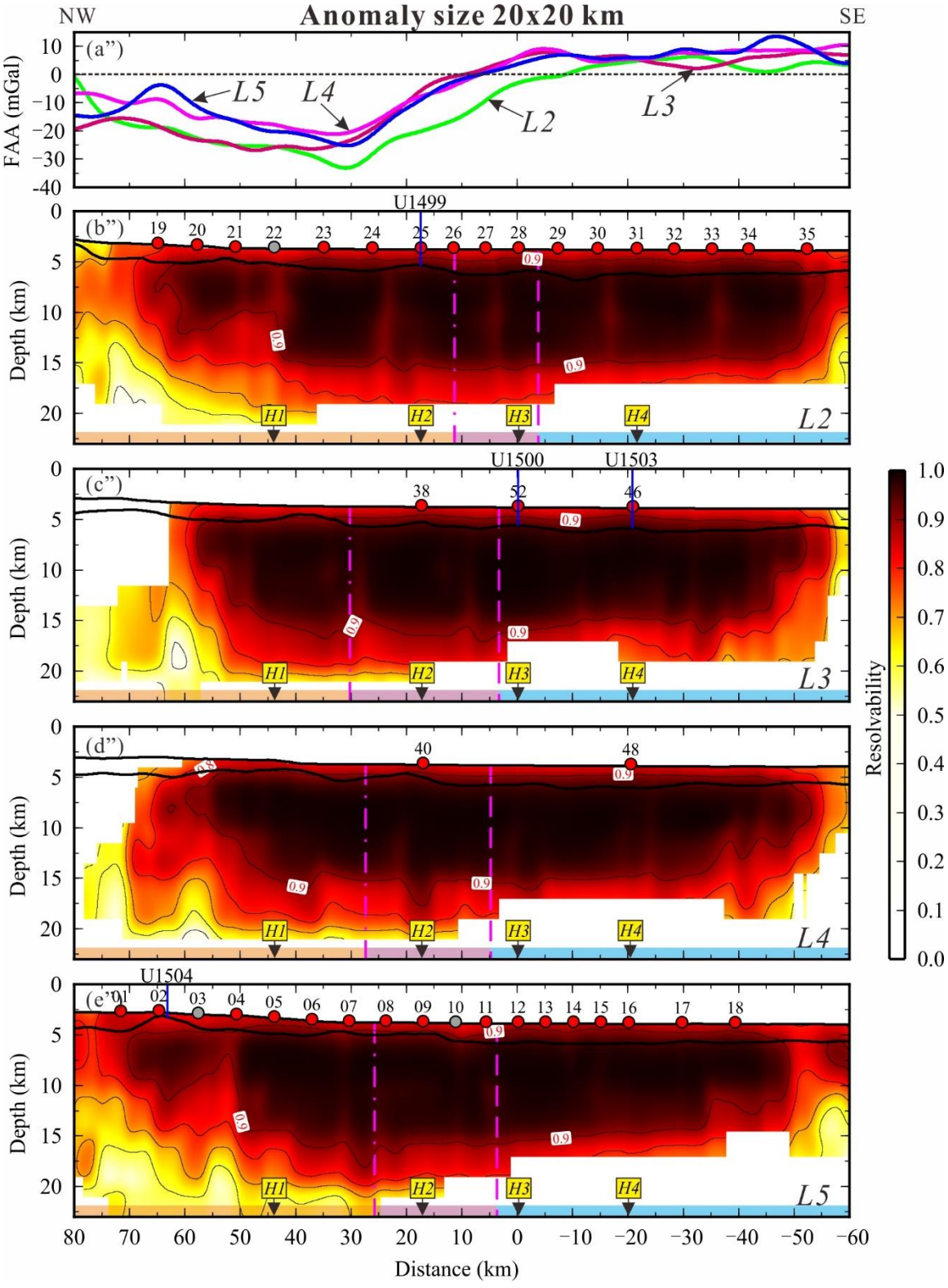

Figure S9 (Continuous).

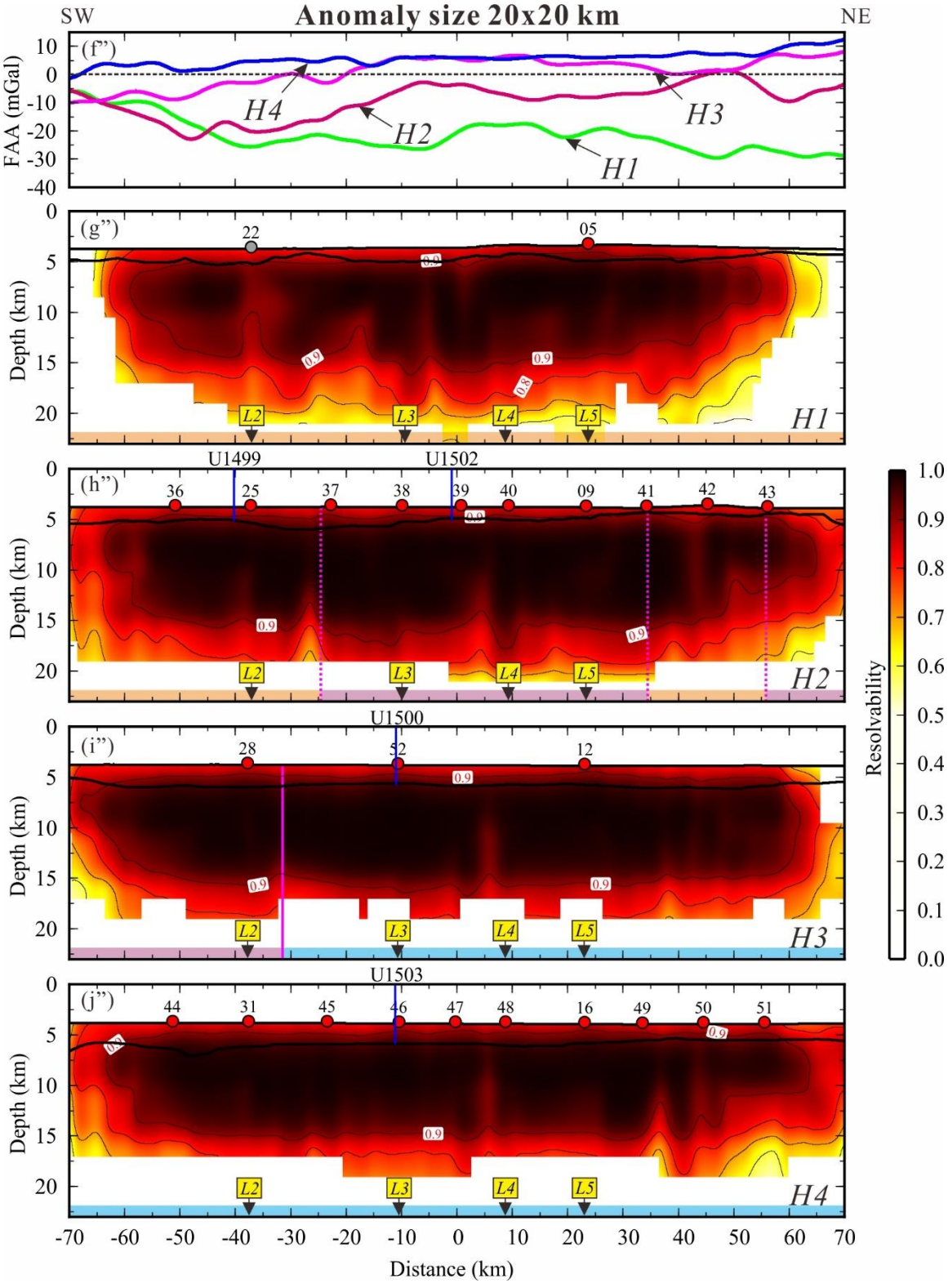

Figure S9 (Continuous).

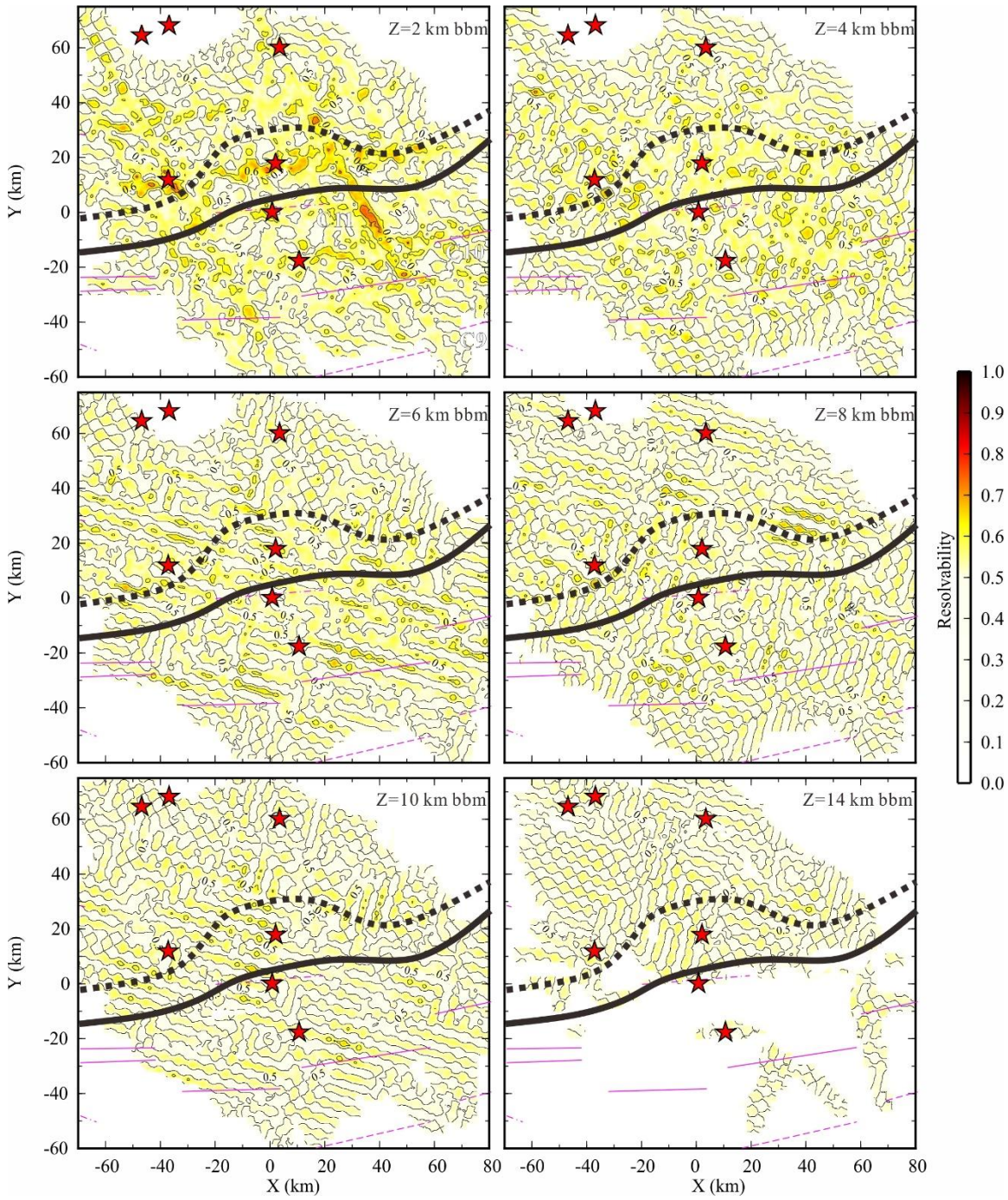

Figure S10. Horizontal slices of the 3D resolvability models with retrieved checkerboard pattern of the 4x4 km, 10x10 km and 20x20 km anomaly size at different depths below sea level (bsl). The other symbols are same as Figure 6.

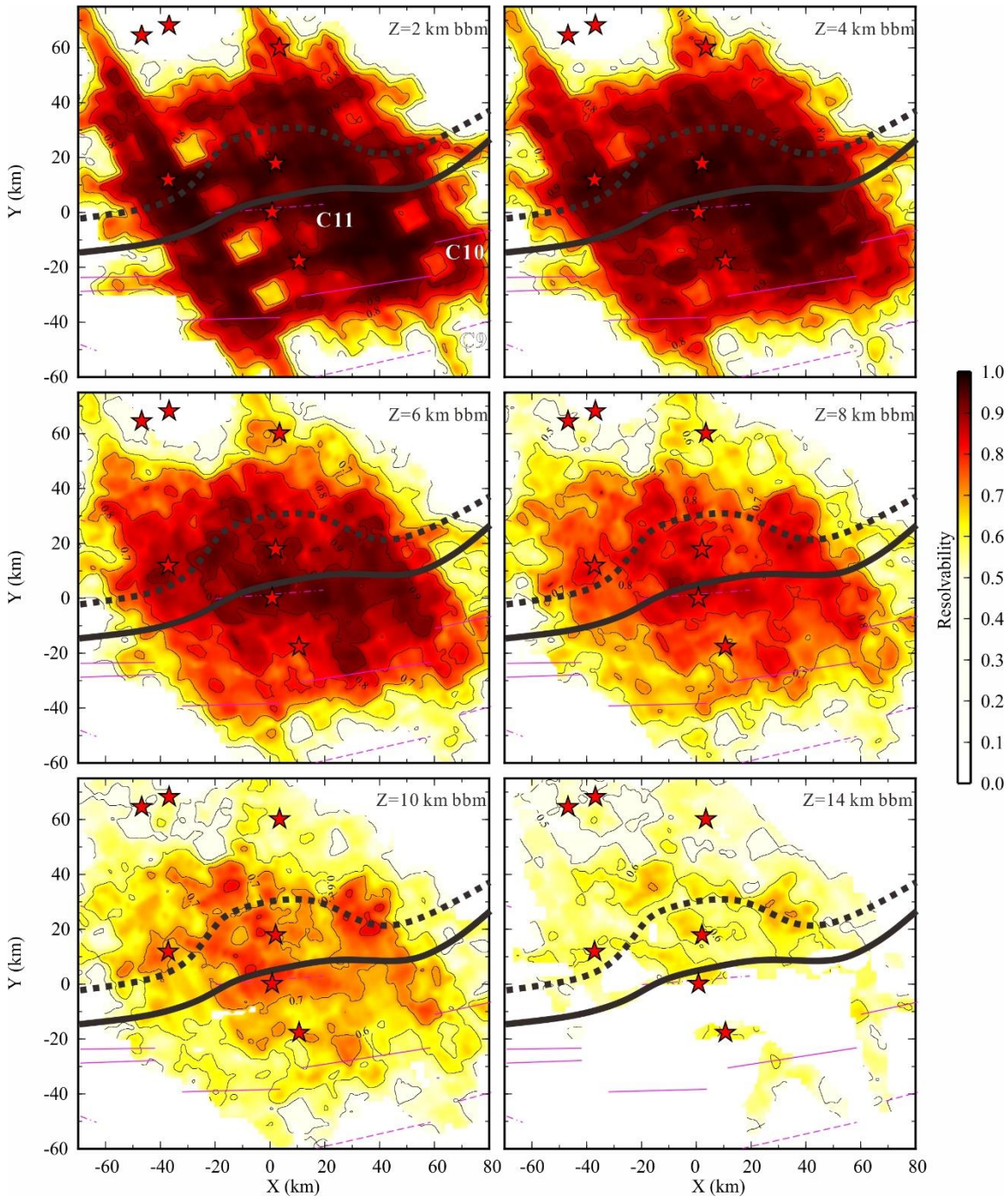

Figure S10 (Continuous).

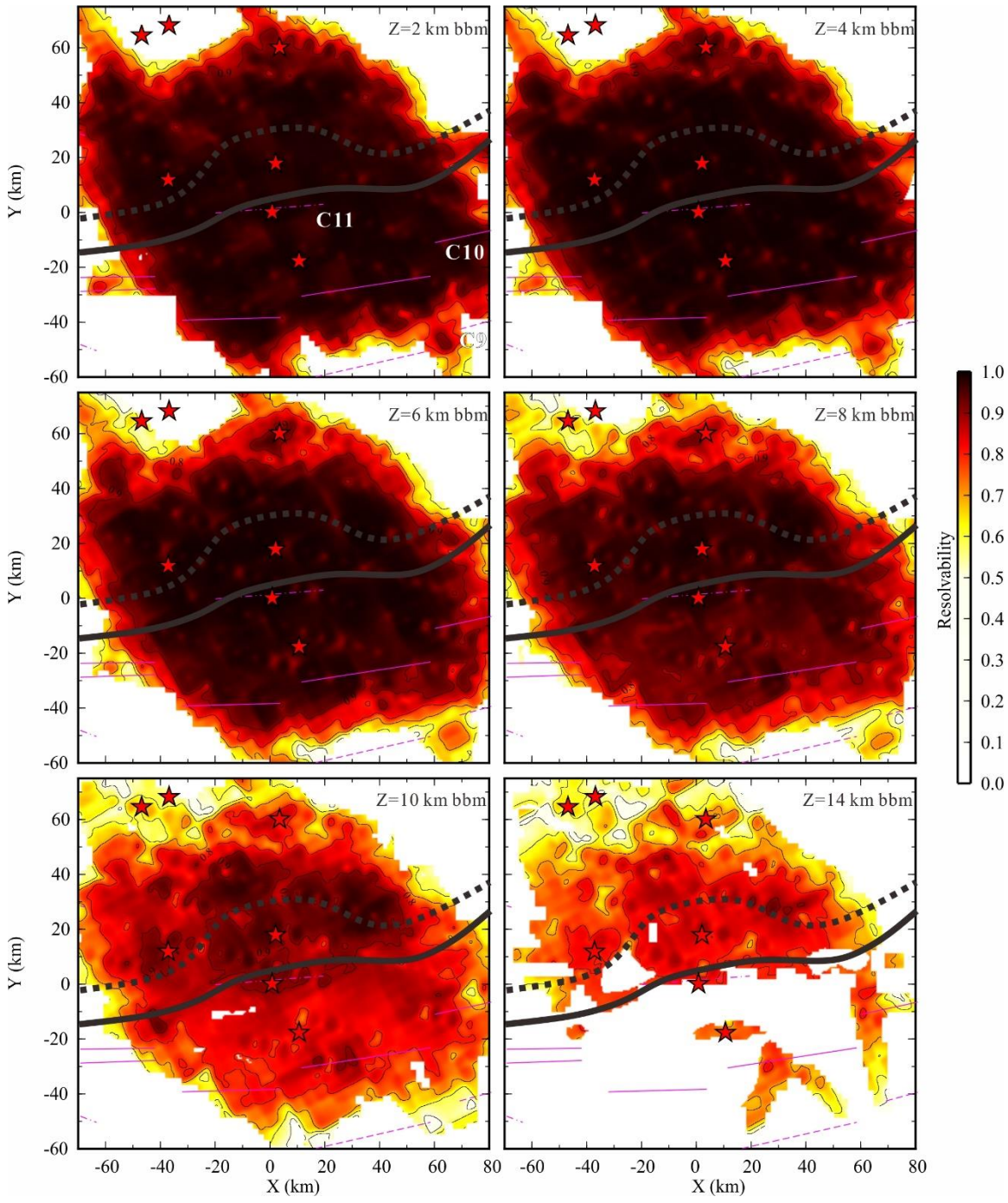

Figure S10 (Continuous).

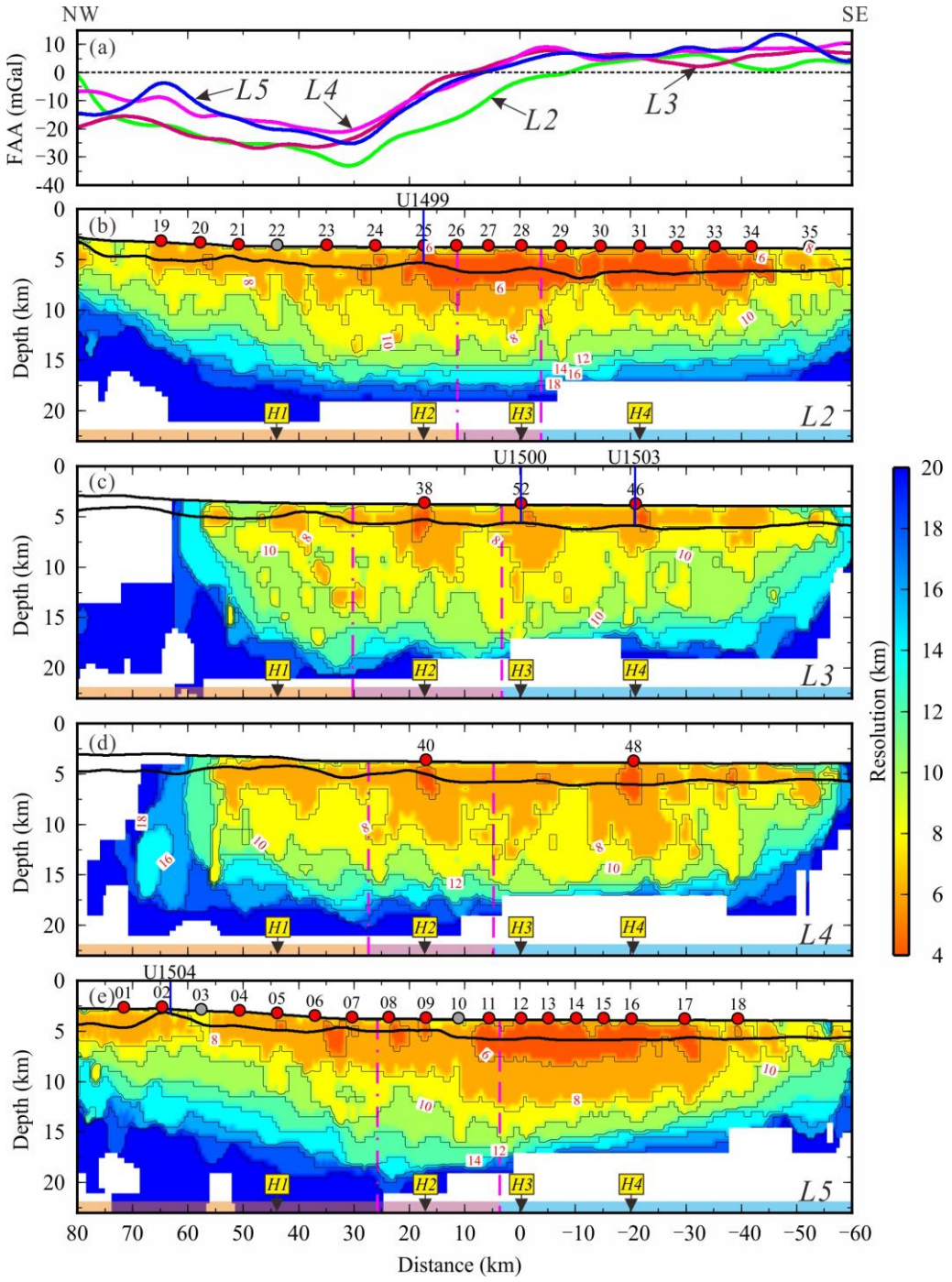

Figure S11. Vertical resolution maps showing the region at which we are able to retrieve each size of the checkerboard pattern. The other markers are same as Figure 5.

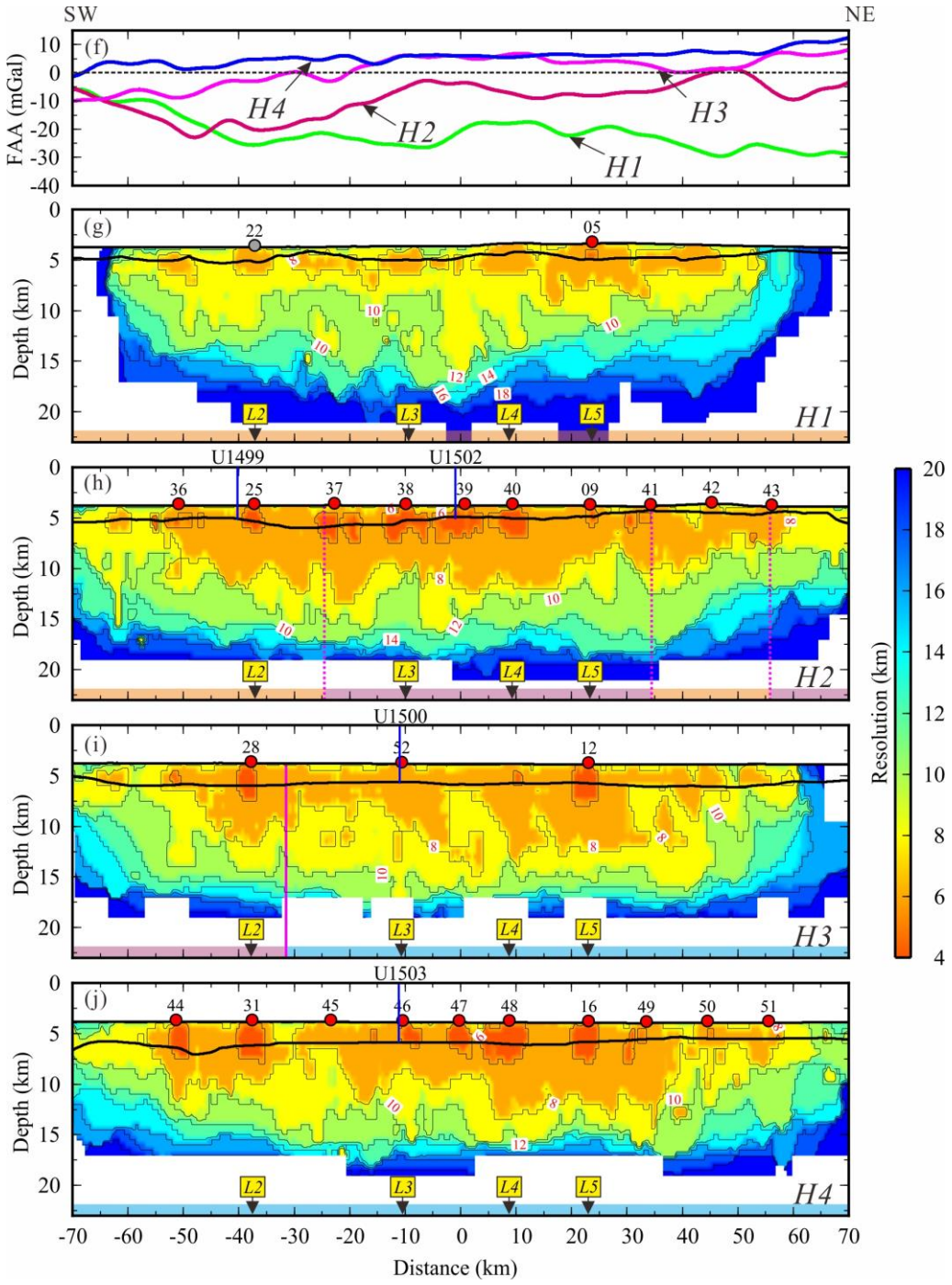

Figure S11 (Continuous).

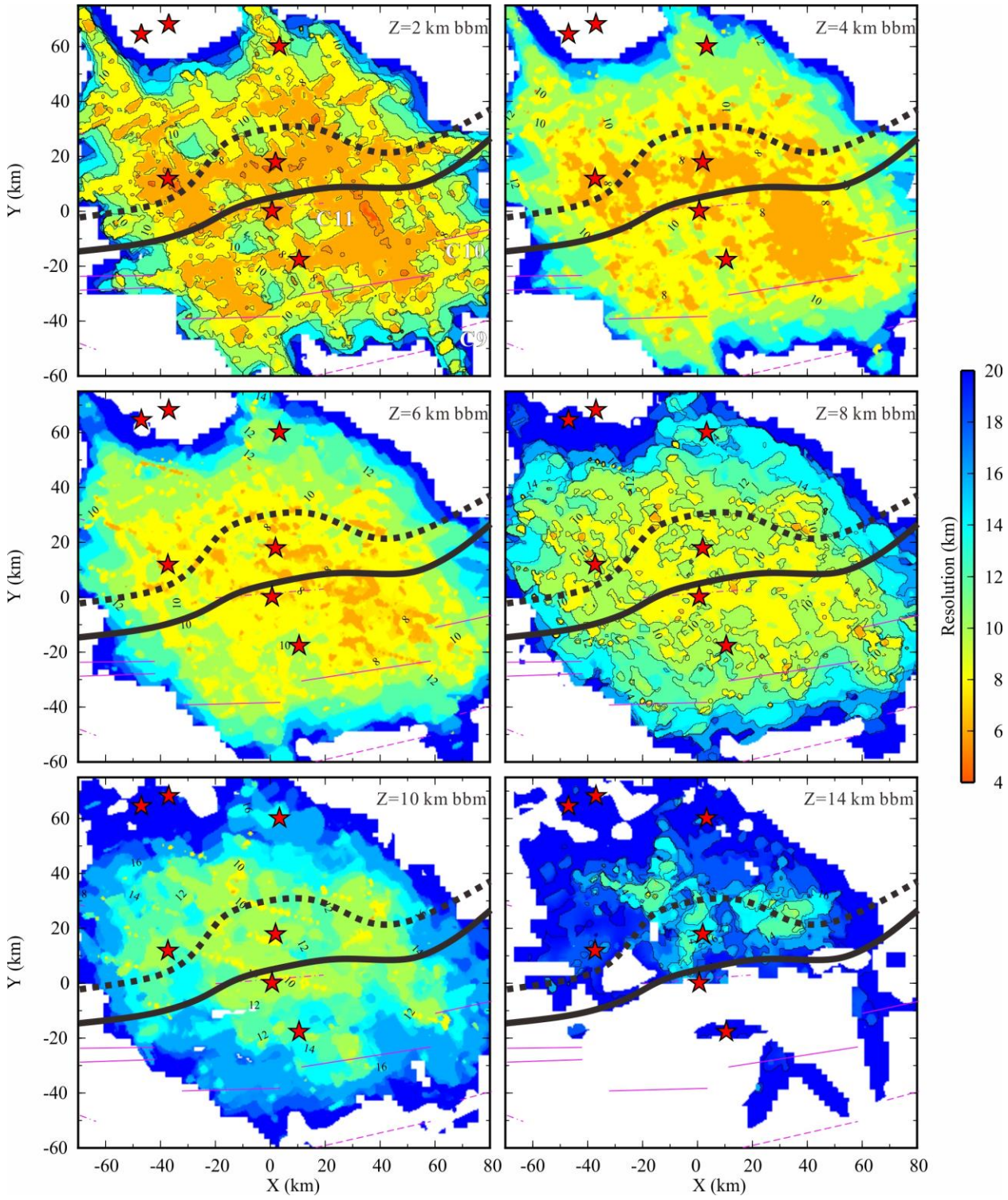

Figure S12. Horizontal resolution maps showing the region at which we are able to retrieve each size of the checkerboard pattern at different depths below TOB (bbm). The other markers are same as Figure 6.

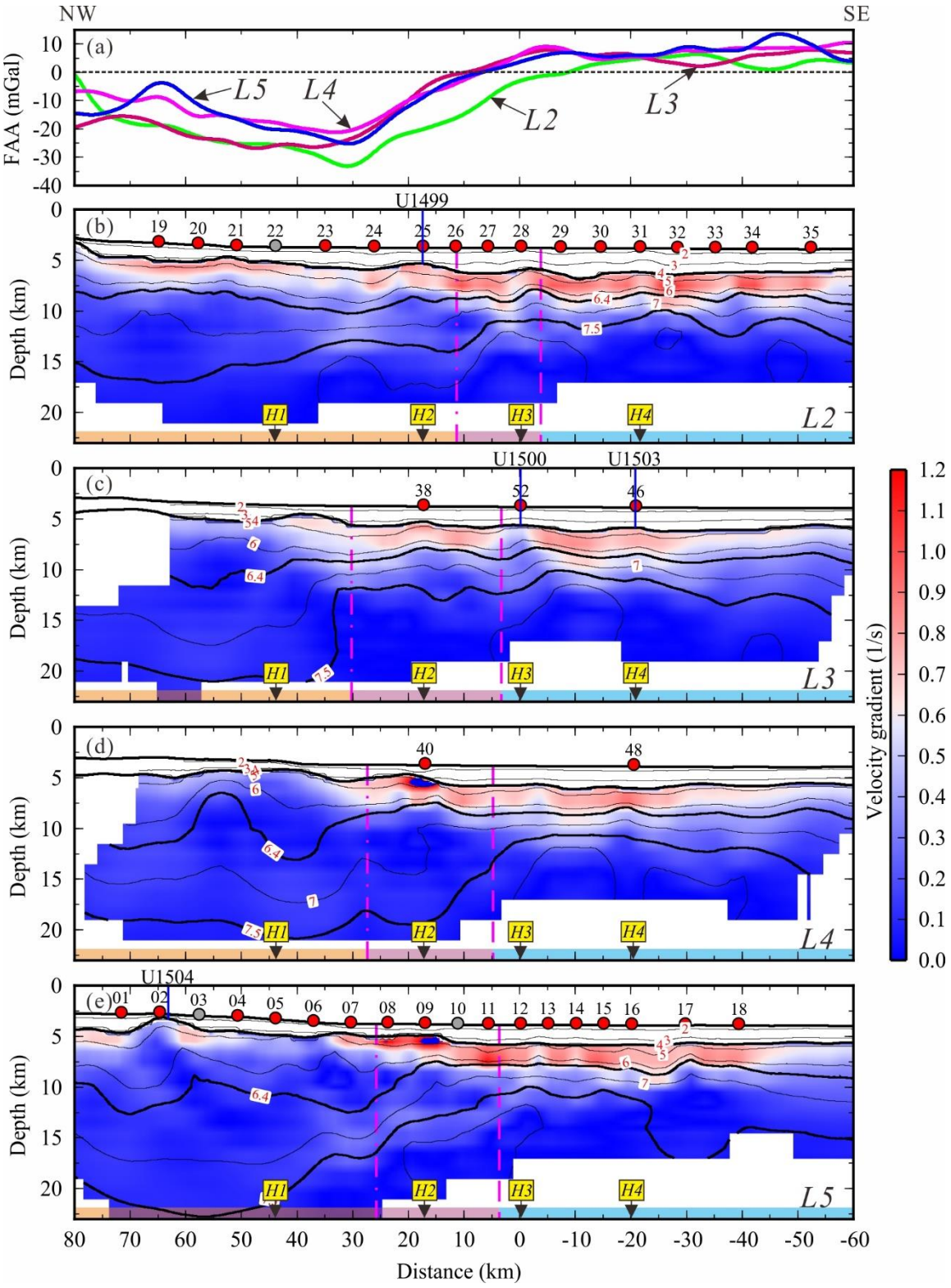

Figure S13. Vertical slices crosscutting the 3D velocity gradient model and free-air gravity anomaly. The other symbols are same as Figure 5.

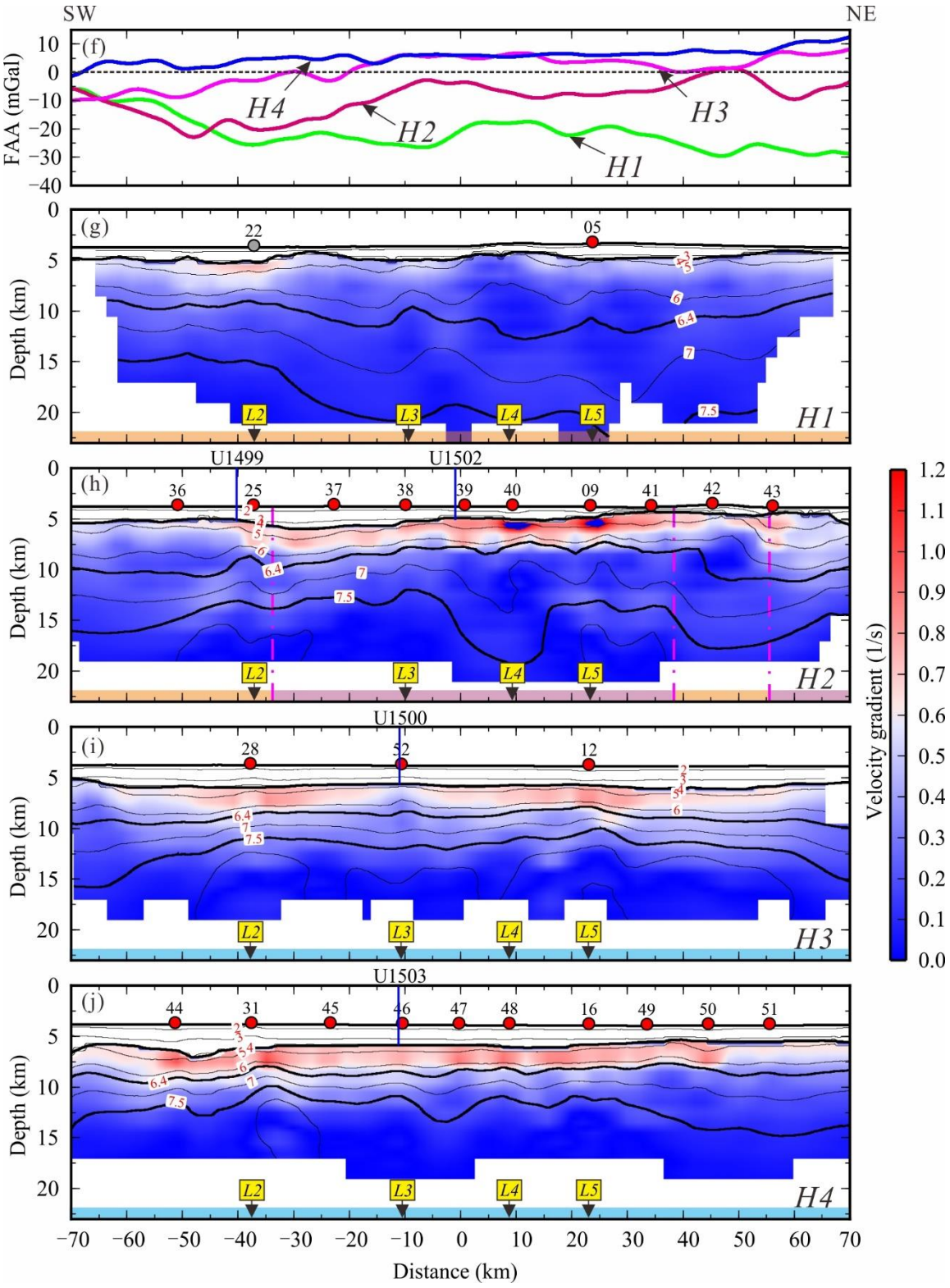

Figure S13 (Continuous).

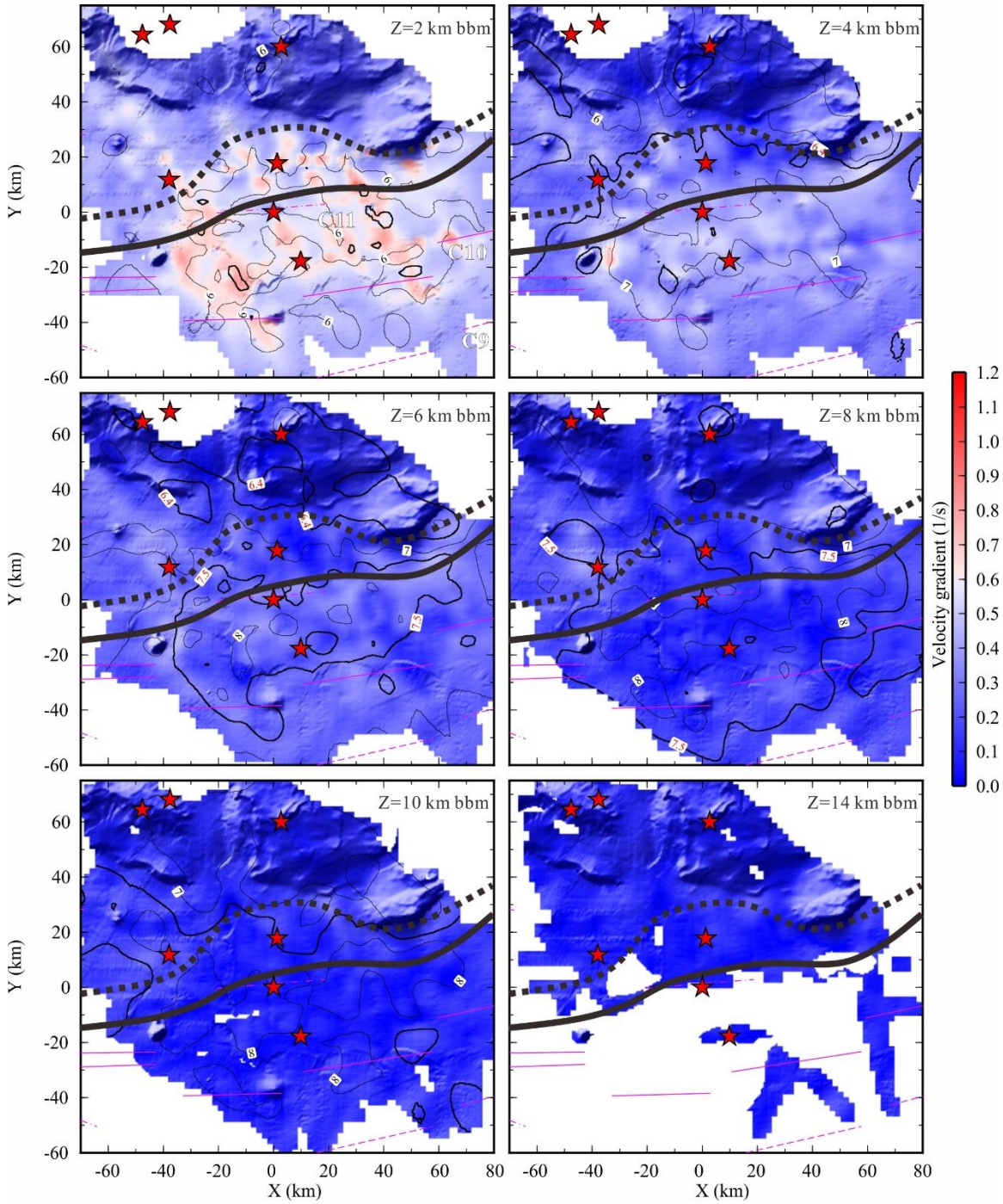

Figure S14. Horizontal slices of the 3D velocity gradient model at different depths below TOB (bbm). The other symbols are same as Figure 6.

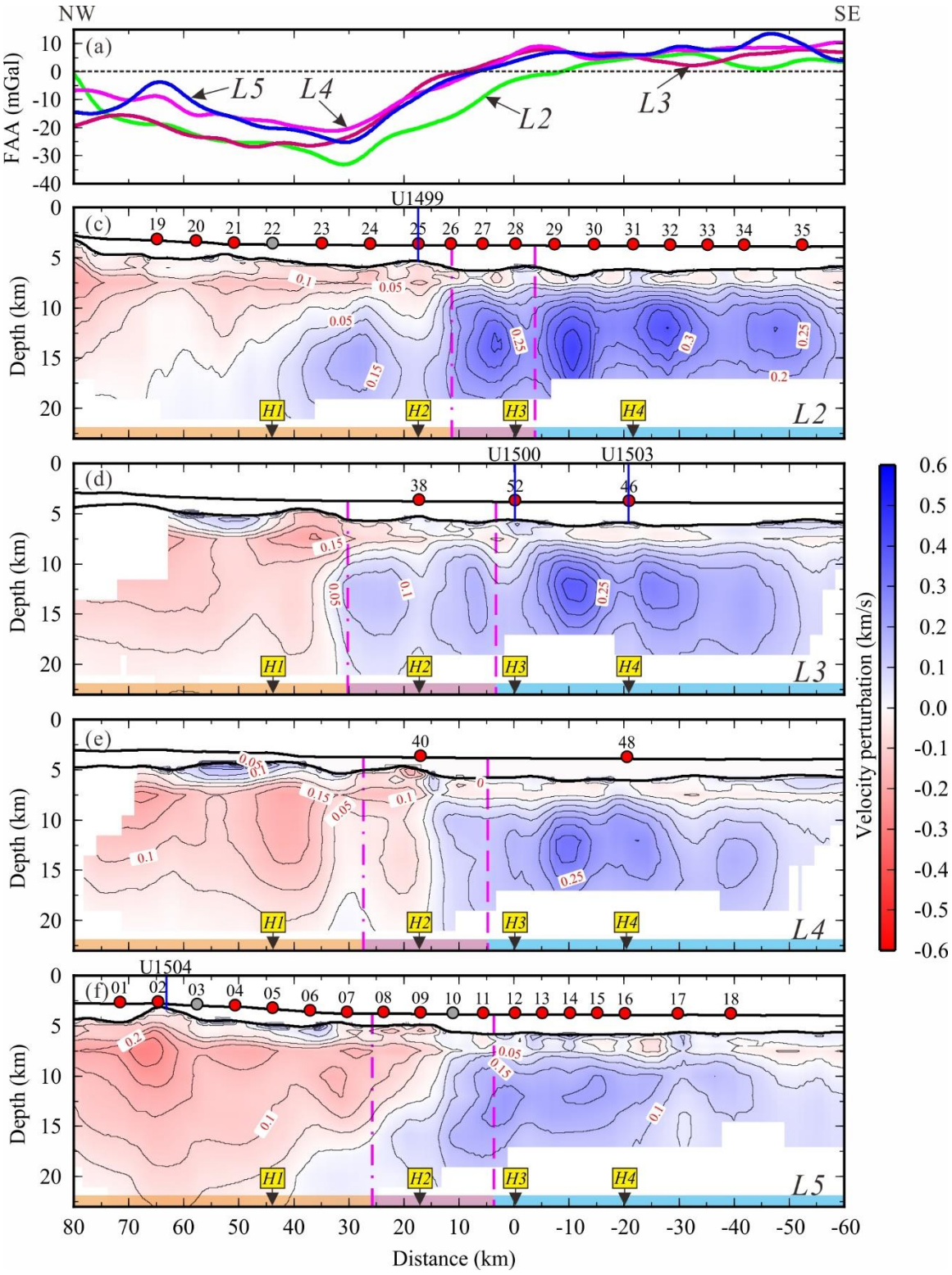

Figure S14. Vertical slices crosscutting the 3D velocity perturbation model and free-air gravity anomaly. The other symbols are same as Figure 5.

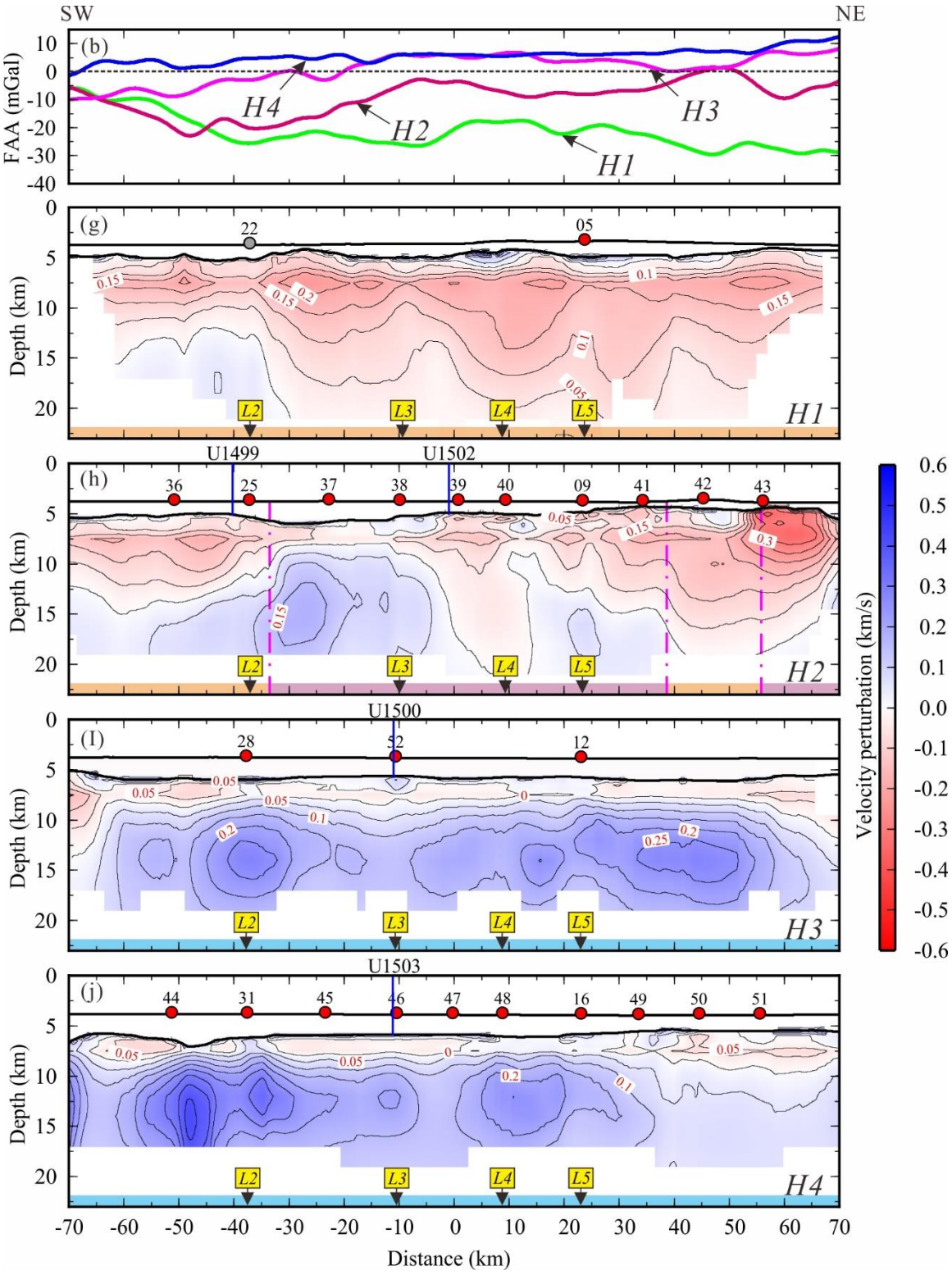

Figure S15 (Continuous).

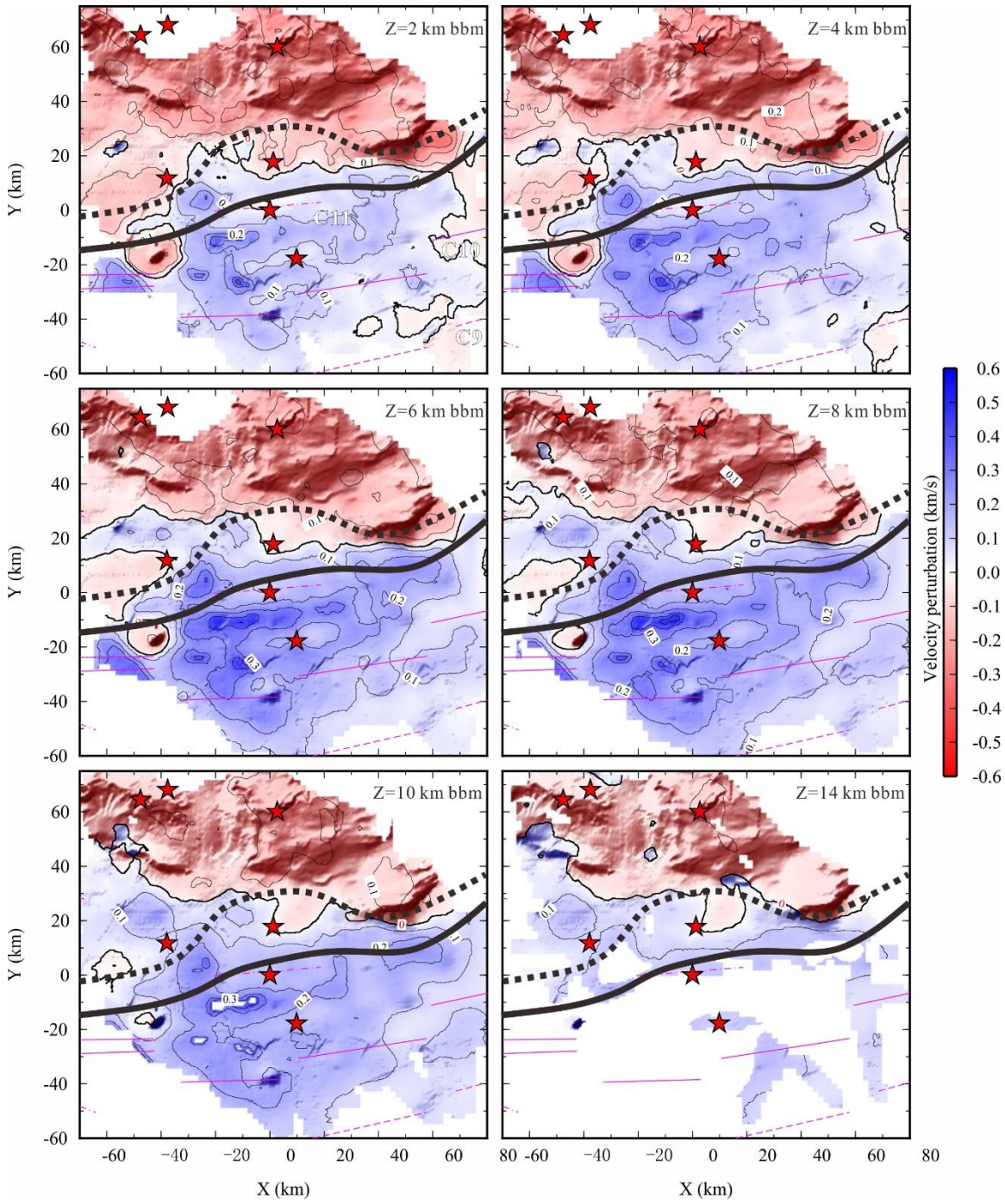

Figure S16. Horizontal slices of the 3D velocity perturbation model at different depths below TOB (bbm). The other symbols are same as Figure 6.

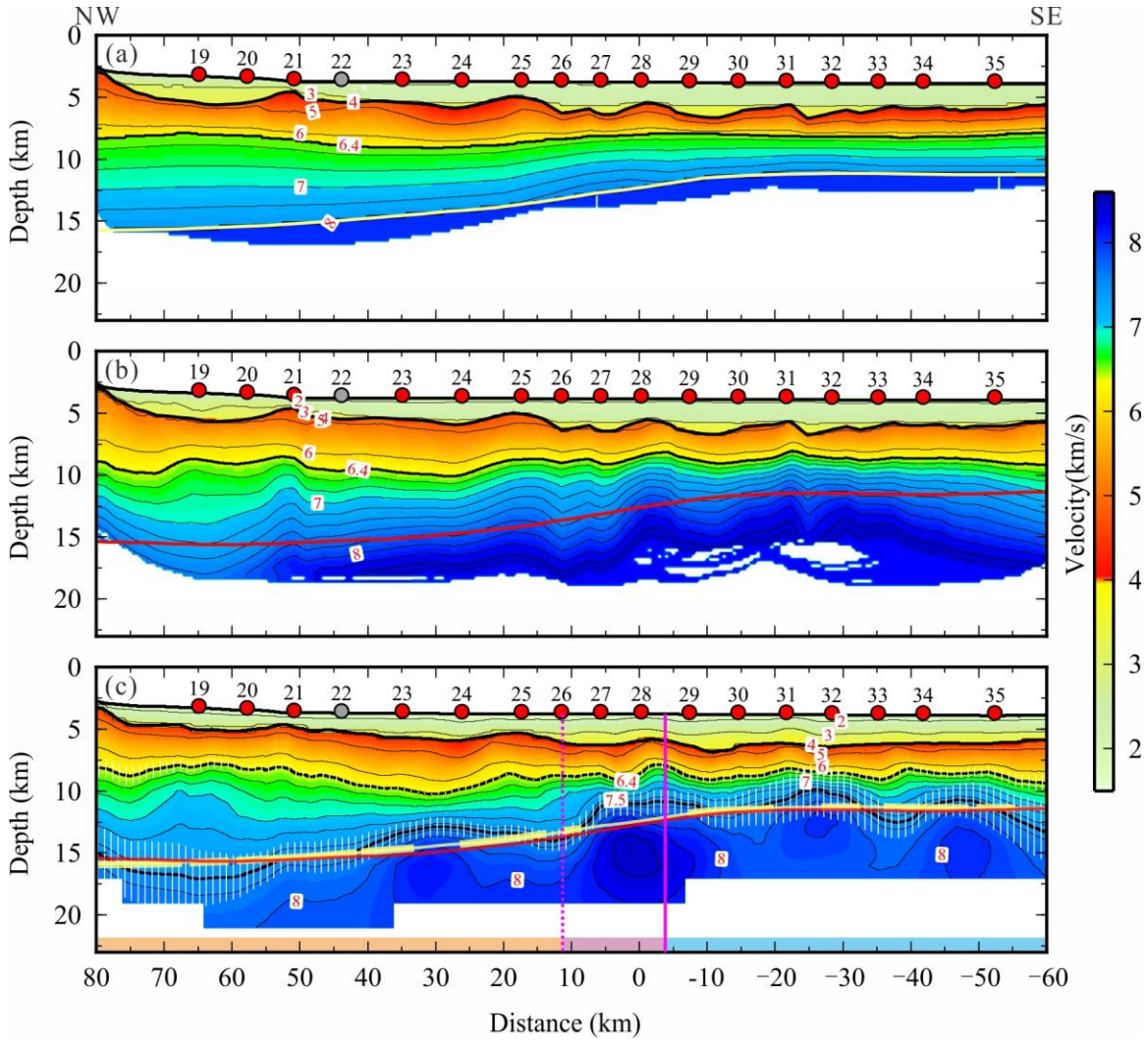

Figure S17. Comparison among (a) Forward Vp model by using RayInvr with the yellow line indicating the inverted Moho; (b) Inversion Vp model by using Tomo2D with the red line showing the inverted Moho; (c) Vertical slice from 3D Vp model along profile L2 with the yellow and red lines from (a) and (b) which correspond well with the 7.5 km/s velocity contour. The white bars show the depth uncertainties for 6.4 km/s and 7.5 km/s contours. The other symbols are same as Figure 5.

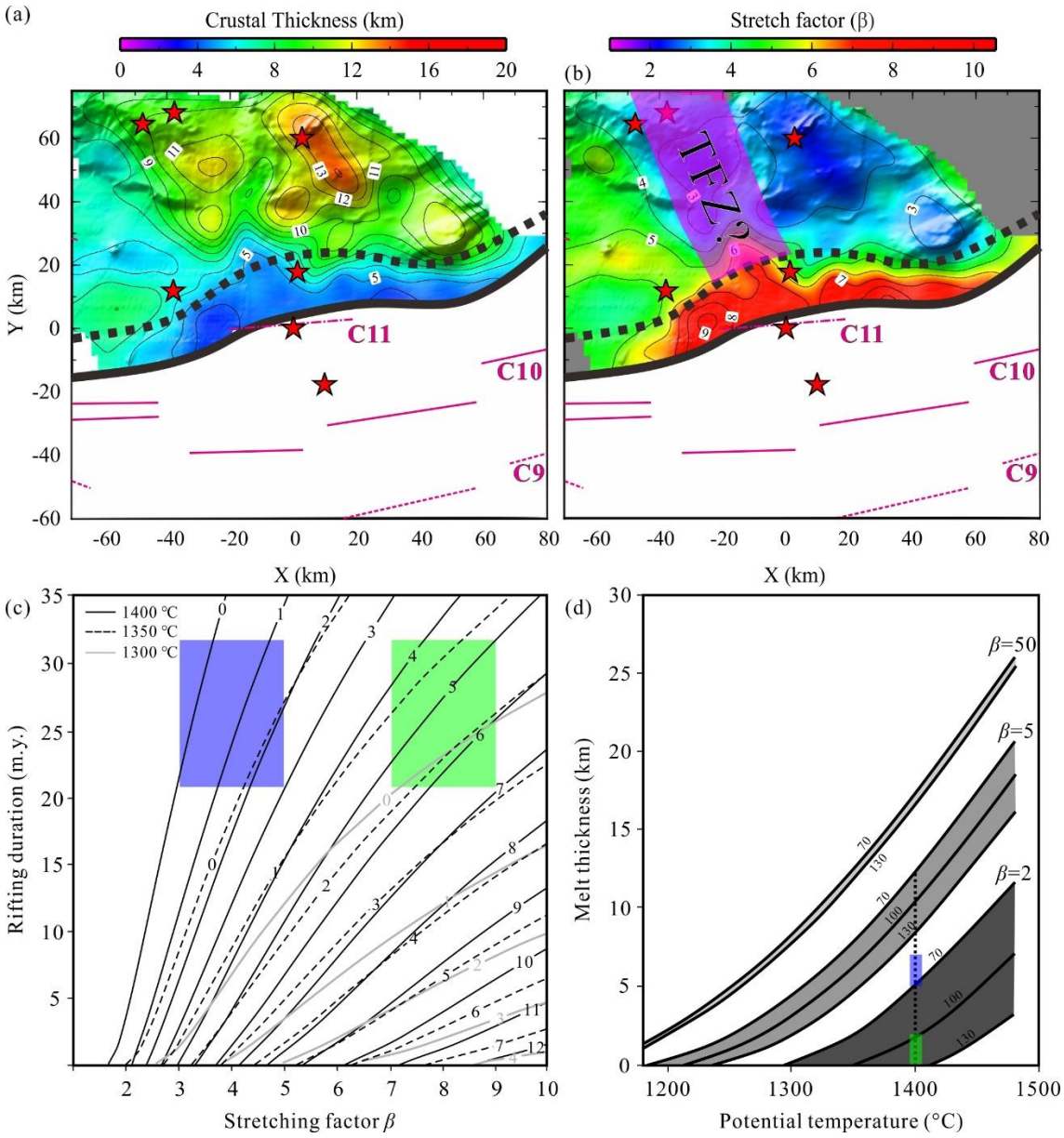

Figure S18. Analysis for the formation genesis of HVLC assuming that it is formed by syn-rift decompression melting of upwelling asthenosphere. (a) The whole crust thickness map removing the HVLC. (b) The whole crustal stretching factor (β) map assuming 32 km as the initial thickness (Li et al., 2006). (c) The relationship among melt thickness, β, rift duration and potential temperature of asthenosphere assuming 125 km as the initial continental lithospheric thickness (modified from Bown et al., 1995). The green and blue rectangles correspond to the SW and NE segments of continental domain, respectively, which are contrary to the observed HVLC thickness in Figure 7d. (d) The relationship among melt thickness, β, potential temperature of asthenosphere and initial continental lithospheric thickness assuming instantaneous breakup (modified from White & McKenzie, 1989). The green and blue thick lines correspond to the melt thickness inferred from HVLC in the SW and NE segments of continental domain, respectively. It can be seen that if the potential temperature of the asthenosphere is uniform of 1400 ℃, the initial lithospheric thickness in NE segment should be smaller than 70 km assuming its β as 2, whereas the initial lithospheric thickness in SW segment should be larger than 260 km assuming its β as 5.